Coronal mass ejections and other extreme characteristics of the 2003 October–November solar eruptions

N. Gopalswamy,[1] S. Yashiro,[1,2] Y. Liu,[3] G. Michalek,[1,2,4] A. Vourlidas,[5] M. L. Kaiser,[1] and R. A. Howard[5]

Received 5 December 2004; revised 3 May 2005; accepted 13 May 2005; published 17 September 2005.

[1] Fast coronal mass ejections (CMEs), X-class flares, solar energetic particle (SEP) events, and interplanetary shocks were abundantly observed during the episode of intense solar activity in late October and early November 2003. Most of the 80 CMEs originated from three active regions (NOAA ARs 484, 486, and 488). We compare the statistical properties of these CMEs with those of the general population of CMEs observed during cycle 23. We find that (1) the 2003 October–November CMEs were fast and wide on the average and hence were very energetic, (2) nearly 20 percent of the ultrafast CMEs (speed $\geq$2000 km s^{-1}) of cycle 23 occurred during the October–November interval, including the fastest CME of the study period ($\sim$2700 km s^{-1} on 4 November 2003 at 1954 UT), (3) the rate of full-halo CMEs was nearly four times the average rate during cycle 23, (4) at least sixteen shocks were observed near the Sun, while eight of them were intercepted by spacecraft along the Sun-Earth line, (5) the CMEs were highly geoeffective: the resulting geomagnetic storms were among the most intense of cycle 23, (6) the CMEs were associated with very large SEP events, including the largest event of cycle 23. These extreme properties were commensurate with the size and energy of the associated active regions. This study suggests that the speed of CMEs may not be much higher than $\sim$3000 km s^{-1}, consistent with the free energy available in active regions. An important practical implication of such a speed limit is that the Sun-Earth travel times of CME-driven shocks may not be less than $\sim$0.5 day. Two of the shocks arrived at Earth in <24 hours, the first events in $\sim$30 years and only the 14th and 15th documented cases of such events since 1859.

Citation: Gopalswamy, N., S. Yashiro, Y. Liu, G. Michalek, A. Vourlidas, M. L. Kaiser, and R. A. Howard (2005), Coronal mass ejections and other extreme characteristics of the 2003 October–November solar eruptions, *J. Geophys. Res.*, *110*, A09S15, doi:10.1029/2004JA010958.

1. Introduction

[2] The violent solar eruptions occurring from 18 October to 8 November 2003 can be considered as extreme events in terms of both their source properties at the Sun and their heliospheric consequences. The eruptions were accompanied by intense solar flares and coronal mass ejections (CMEs) of very high energy. The plasma, particle, and electromagnetic consequences of these events were detected by various instruments located throughout the heliosphere. Disturbances associated with two of the eruptions arrived at Earth in less than a day, providing benchmark data for space weather purposes. Historically, there were only 13 documented eruptions, with <1-day shock travel time to Earth [*Cliver et al.*, 1990a, 1990b; *Cliver and Svalgaard*, 2004], including the 1 September 1859 event corresponding to the first flare ever reported [*Carrington*, 1860; *Hodgson*, 1860]. The purpose of this study is to obtain the statistical properties of the 2003 October–November CMEs and compare them with those of the general population of CMEs observed during solar cycle 23. This study also places these events in perspective of other large events. We analyze the flares, CMEs, shocks, and SEPs, all of which were linked to the magnetic free energy available in the underlying solar active regions. We also study the travel time of the associated shocks to Earth and the intensity of the consequent geomagnetic storms. We pay particular attention to the three fastest shocks of the study period that were followed by interplanetary CMEs and marked the commencement of intense geomagnetic storms. We finally examine the place of the 2003 October–November active regions among other SEP-producing regions of solar cycle 23.

[1]NASA Goddard Space Flight Center, Greenbelt, Maryland, USA.
[2]Also at Catholic University of America, Washington, D.C., USA.
[3]W.W. Hansen Experimental Physics Laboratory, Stanford University, Stanford, California, USA.
[4]Also at Astronomical Observatory of Jagiellonian University, Krakow, Poland.
[5]Naval Research Laboratory, Washington, D.C., USA.

0148-0227/05/2004JA010958$09.00

2. Observations and Data Sources

[3] The primary data set used in this study is the compilation of white-light CMEs at the CDAW Data Center at

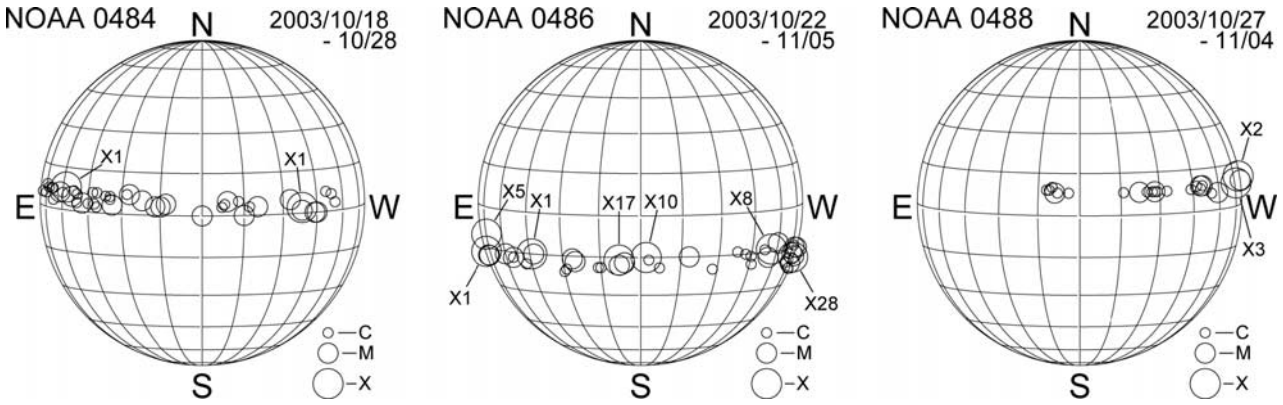

Figure 1. Source locations of C, M, and X-class flares from the three NOAA active regions (484, 486, and 488). The approximate size of the X-class flares are also indicated. The dates during which the flares were observed are shown at the right-hand top corner in each frame.

NASA's Goddard Space Flight Center (http://cdaw.gsfc.nasa.gov/CME_list). This data base contains the measured properties of white light CMEs observed by the Solar and Heliospheric Observatory (SOHO) mission's Large Angle and Spectrometric Coronagraphs (LASCO) [*Brueckner et al.*, 1995]. The solar eruptions originated primarily in three active regions (ARs) with NOAA numbers 484, 486, and 488. Information on the flares and the associated active regions was obtained from the online Solar Geophysical Data (SGD). Shocks associated with solar eruptions are inferred from type II radio bursts. Ground-based observations of metric-wavelength type II bursts were collected from the SGD reports. Decameter-hectometric (DH) type II bursts, which correspond to shocks in the interplanetary (IP) medium, were recorded by the Radio and Plasma Wave (WAVES) [*Bougeret et al.*, 1995] experiment on board the Wind spacecraft. Many of these shocks travel far into the heliosphere and some of them are detected in situ by spacecraft [*Skoug et al.*, 2004]. We used in situ shock data from SOHO's proton monitor (http://umtof.umd.edu/pm/) and ACE spacecraft. The interplanetary CMEs (ICMEs) that follow the shocks were also detected by the ACE spacecraft. ICMEs cause large geomagnetic storms. The intensity of the geomagnetic storms were obtained from the disturbance storm (Dst) index as listed at the World Data Center in Kyoto (http://swdcdb.kugi.kyoto-u.ac.jp/dstdir/). The CMEs were also associated with large solar energetic particle (SEP) events. Information on the SEP events were gathered from the online SGD.

3. Flares

[4] We selected all the GOES C, M, and X-class flares from ARs 484, 486, and 488. Source regions of all the X-class flares were listed in the SGD. A few M-class flares and a sizable number of C-class flares reported in the SGD did not have source locations reported in the SGD; by playing movies of EUV images obtained by SOHO's Extreme-Ultraviolet Imaging Telescope (EIT), we were able to identify the heliographic locations of these flares. These movies, with a typical cadence of $\sim$12 min, show most of the eruptions either in direct images or in running difference images. We also made use of the Solarsoft data archive (http://www.lmsal.com/solarsoft/last_events/) to confirm flare locations. Figure 1 shows the source locations of the flares from the three active regions, the size of the data point indicating the flare size (small, medium, and large circles denoting C, M, and X-class flares, respectively). The activity started on 18 October 2003 when AR 484 was at the east limb and continued until 8 November 2003 when AR 486 was behind the west limb. This interval is chosen to be our study period, which we refer to as the "Oct/Nov 03 period" and the events as the "Oct/Nov 03 events." The flares from AR 484 were observed between 18 and 26 October. AR 486 was the most active of the three regions and produced flares over the entire duration of its disk passage (22 October to 5 November) and beyond (as inferred from CMEs). AR 488 emerged during the study period and produced its first flare on 27 October when it was at N09E11. This region also produced flares until it rotated behind the west limb on 4 November. In all, there were 143 well-defined flares from the three active regions (54 from AR 484; 60 from AR 486; 29 from AR 488). ARs 484 and 488 each produced two X-class flares whereas AR 486 produced seven X-class flares including the largest flare of the solar cycle on 4 November 2003 (GOES X-ray class >X28).

4. CMEs

[5] A total of 80 CMEs were observed during the study period, compared with the 143 flares (GOES X-ray C-class and above) over the same period. Most of the CMEs originated from the three active regions. The actual number of CMEs is expected to be larger because some of the narrower CMEs erupting from close to the disk center are not likely to be observed by the coronagraphs [see *Gopalswamy et al.*, 2001a]. All the observed CMEs are listed in Table 1 with date, time of first appearance in the LASCO field of view, speed (V in km s^{-1}), width (W in degrees), mass (M in g), and kinetic energy (KE in ergs) in columns 2–7, respectively. The speed and width were measured in the sky plane, so they are expected to be lower limits to the actual values. The speeds were obtained by a

Table 1. Characteristics of CMEs Observed During the 2003 October–November Period[a]

	CME					Flare			NOAA
Number	Date/Time	V	W	M	KE	Time	Class	Location	AR
1	2003/10/18 0554	707	10	1.1e+14	2.8e+29	0531	C2.0	N05E80	484
2	2003/10/18 0731	397	24	2.0e+14	1.6e+29	—	—	Backside	—
3	2003/10/18 0907	778	12	1.8e+14	5.6e+29	0849	C3.3	N05E75	484
4	2003/10/18 1530	627	360	7.2e+15	1.4e+31	—	—	SE90b	486-
5	2003/10/18 2059	652	54	2.5e+15	5.3e+30	2026	C3.3	N06E70	484
6	2003/10/18 2130	309	85	4.0e+14	1.9e+29	—	—	Backside	—
7	2003/10/18 2130	509	136	6.0e+15	7.8e+30	—	—	SE90b	486-
8	2003/10/18 2355	544	114	5.9e+15	8.8e+30	—	—	E90b	486-
9	2003/10/19 0654	798	38	2.7e+14	8.7e+29	0608	M1.9	N07E65	484
10	2003/10/19 0830	469	53	8.6e+14	9.5e+29	—	—	N06E64?	484?
11	2003/10/19 1708	472	150	7.2e+15	8.1e+30	1629	X1.1	N06E61	484
12	2003/10/19 1952	799	113	1.3e+15	4.2e+30	—	—	SE90b	486-
13	2003/10/19 2230	469	23	3.2e+14	3.5e+29	—	—	W90b	—
14	2003/10/21 0354	1484	360	1.2e+16	1.3e+32	—	—	SE90b	486-
15	2003/10/21 1606	533	24	7.7e+14	1.1e+30	—	—	SE90b	486?
16	2003/10/21 1954	720	47	5.9e+15	1.5e+31	1922	M1.?	S16E90	486
17	2003/10/21 2058	602	75	6.5e+15	1.2e+31	2150	M1.?	S17E90	486
18	2003/10/21 2330	824	39	8.3e+14	2.8e+30	2300	M2.4	S17E90	486
19	2003/10/22 0131	666	54	3.8e+15	8.3e+30	0125	C9.?	S13E90	486
20	2003/10/22 0354	1163	101	5.8e+15	3.9e+31	0328	M3.7	S13E88	486
21	2003/10/22 0830	719	267	1.1e+16	2.8e+31	—	—	N07E25?	484?
22	2003/10/22 1530	1054	18	—	—	1506	M1.4	N04E29	484
23	2003/10/22 1630	1040	23	—	—	1557	M1.2	N05E29	484
24	2003/10/22 2006	1085	134	9.7e+15	5.7e+31	1947	M9.9	S17E88	486
25	2003/10/23 0306	656	46	6.4e+14	1.4e+30	0235	M2.4	N03E15	484
26	2003/10/23 0731	1090	20	—	—	0702	M3.2	N04E13	484
27	2003/10/23 0854	1406	236	1.2e+16	1.2e+32	0819	X5.4	S18E88	486
28	2003/10/23 1354	511	36	8.1e+14	1.1e+30	—	—	S11W90	—
29	2003/10/23 2006	1136	95	1.1e+16	7.2e+31	1950	X1.1	S17E88	486
30	2003/10/24 0254	1055	123	1.2e+16	6.9e+31	0227	M7.6	S17E72	486
31	2003/10/24 0530	1233	44	1.0e+15	7.9e+30	0504	M4.2	S24E74	486
32	2003/10/24 1630	384	88	2.1e+15	1.5e+30	1523	C8.9	S19E60	486
33	2003/10/24 2006	399	38	1.0e+15	8.2e+29	1842	M1.3	S19E68	486
34	2003/10/25 0518	685	113	4.4e+15	1.0e+31	0417	M1.2	S14E45	486
35	2003/10/25 0830	235	51	1.4e+14	3.8e+28	—	—	Backside	—
36	2003/10/26 0131	419	75	2.8e+15	2.4e+30	—	—	S17W62	483
37	2003/10/26 0530	684	86	7.2e+15	1.7e+31	—	—	S01W60	483
38	2003/10/26 0654	1371	207	1.2e+16	1.2e+32	0557	X1.2	S15E43	486
39	2003/10/26 0830	258	96	1.4e+16	4.5e+30	—	—	Backside	—
40	2003/10/26 1034	929	27	1.0e+14	4.4e+29	—	—	Backside?	—
41	2003/10/26 1754	1537	171	2.0e+16	2.4e+32	1721	X1.2	N04W43	484
42	2003/10/27 0430	481	48	2.4e+15	2.8e+30	0412	M1.2	N00W44	484
43	2003/10/27 0506	323	24	2.0e+14	1.1e+29	—	—	S15E30?	486?
44	2003/10/27 0830	1322	144	4.5e+15	3.9e+31	0751	M2.7	N00W48	484
45	2003/10/27 1331	1005	45	4.1e+14	2.1e+30	1227	M6.7	N06W45	484
46	2003/10/27 2030	990	43	9.5e+14	4.7e+30	1948	C9.0	N06W49	484
47	2003/10/28 0554	602	17	—	—	0507	C7.7	N06W53	484
48	2003/10/28 0630	684	15	1.6e+14	3.8e+29	—	—	N06W51	484
49	2003/10/28 0731	394	16	—	—	—	—	S17E19?	486?
50	2003/10/28 0930	853	22	1.5e+15	5.5e+30	—	—	E90b	—
51	2003/10/28 1054	1054	147	1.1e+15	6.1e+30	1018	M8.?	S16E15	486
52	2003/10/28 1130	2459	360	4.0e+16	1.2e+33	1100	X17.	S20E02	486
53	2003/10/29 1016[a]	922	114	1.6e+17	7.0e+32	—	—	—	486?
54	2003/10/29 2054	2029	360	1.6e+16	3.4e+32	2037	X10.	S19W09	486
55	2003/10/31 0442	2126	50	7.1e+14	1.6e+31	0426	M2.0	N06W90	484
56	2003/10/31 0702	62	44	7.5e+14	1.4e+28	—	—	—	—
57	2003/10/31 1730	309	34	8.8e+14	4.2e+29	1644	C5.3	S17W47	486
58	2003/10/31 2030	605	10	6.7e+13	1.2e+29	—	—	N01E63	—
59	2003/11/01 1230	246	68	1.6e+15	4.7e+29	—	—	—	—
60	2003/11/01 1454	334	55	7.5e+15	4.2e+30	—	—	—	—
61	2003/11/01 2130	413	143	4.9e+15	4.2e+30	—	—	W90b	484+
62	2003/11/01 2306	899	93	8.9e+15	3.6e+31	2226	M3.2	S12W60	486
63	2003/11/02 0930	2036	360	4.5e+16	9.3e+32	—	—	Backside	484?
64	2003/11/02 1730	2598	360	4.9e+15	1.6e+32	1703	X8.3	S18W59	486
65	2003/11/03 0159	827	65	6.6e+15	2.3e+31	0109	X2.7	N08W73	488
66	2003/11/03 1006	1420	103	1.3e+16	1.3e+32	0943	X3.9	N08W78	488
67	2003/11/03 1931	641	26	2.0e+14	4.2e+29	—	—	E90b	—
68	2003/11/04 1206	1208	360	1.1e+16	8.3e+31	—	—	Backside	—
69	2003/11/04 1254	605	72	2.3e+15	4.2e+30	—	—	S21W88	486
70	2003/11/04 1931	327	52	3.5e+15	1.9e+30	—	—	Backside	—
71	2003/11/04 1954	2657	360	1.7e+16	6.1e+32	1929	X28.	S18W88	486
72	2003/11/05 1654	1075	12	3.0e+14	1.7e+30	—	—	W90b	491+

Table 1. (continued)

	CME					Flare			NOAA
Number	Date/Time	V	W	M	KE	Time	Class	Location	AR
73	2003/11/06 0354	532	12	7.9e+13	1.1e+29	—	—	SE90b	—
74	2003/11/06 0406	643	23	3.9e+14	8.0e+29	—	—	W90b	—
75	2003/11/06 0430	301	21	3.8e+13	1.7e+28	—	—	W90b?	486?
76	2003/11/06 0731	749	11	2.0e+14	5.7e+29	—	—	SE90b	—
77	2003/11/06 1730	1523	360	1.3e+16	1.6e+32	—	—	Backside	—
78	2003/11/07 1554	2237	360	9.9e+15	2.5e+32	—	—	W90b	486+
79	2003/11/08 0654	656	71	3.4e+14	7.4e+29	—	—	E90b	—
80	2003/11/08 0930	703	44	7.7e+14	1.9e+30	—	—	SW90b	495

[a]It was possible to measure the speeds of all but one of the 80 CMEs. The 29 October 2003 at 1016 UT (probably from AR 486) occurred when the "snow storm" caused by the big halo CME on 28 October was in progress. The CME was not seen in the C2 images but was seen in C3 images. The speed was estimated to be about 922 km s^{-1}, but the value is not reliable.

straight-line fit to the height-time measurements and hence are average values within the LASCO field of view (~2–32 Rs). The onset time, GOES X-ray class, and the heliographic location of the associated flares are listed in columns 8–10. The last column lists the NOAA number of the associated active region. Completely backside CMEs are indicated by "Backside" in column 10. It was difficult to estimate the angle behind the limb for these events. A subscript "b" to the entries in column 10 denotes that the eruption occurred behind the specified limb. For example, "SE90b" means the eruption occurred behind the SE limb. The minus and plus signs after the NOAA number indicates that the region was just behind the east and west limb, respectively.

[6] As Table 1 shows, the largest number of CMEs (32) and the most energetic ones originated from AR 486. Figure 2 shows snapshots of several large CMEs from AR 486. One can see that the central position angles of the CMEs change from SE to SW because the active region was located at a latitude of S15. For the two full halo CMEs of 28 and 29 October, no position angle could be defined. However, the height-time measurements were

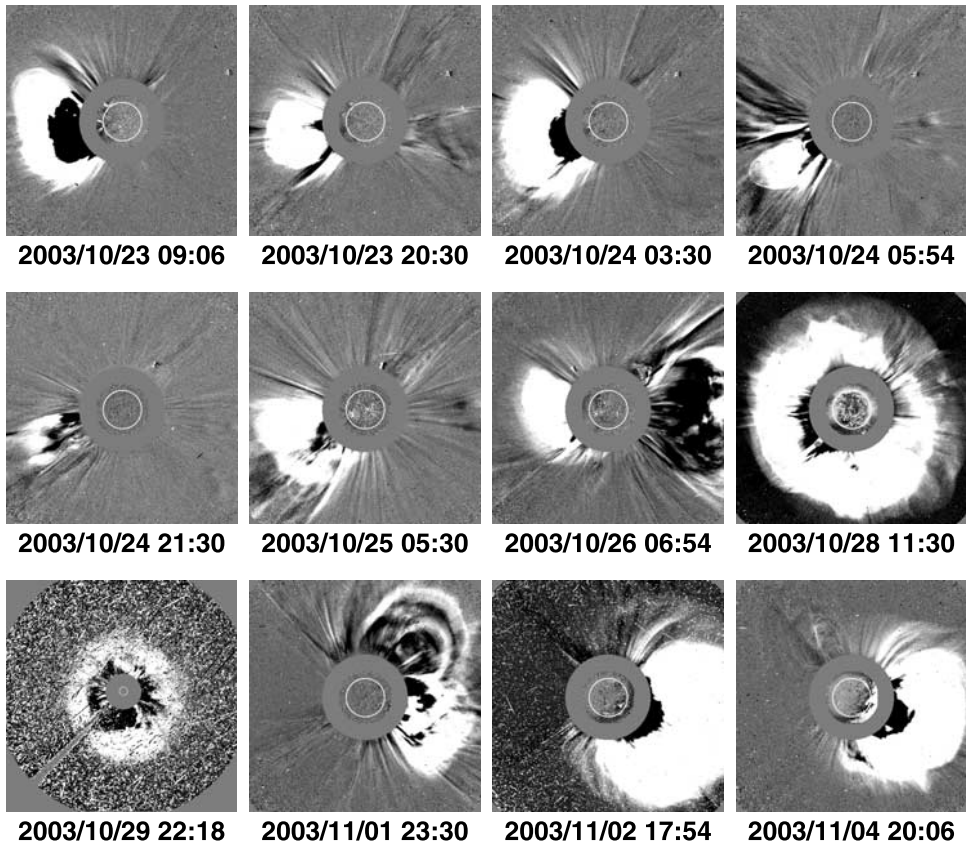

Figure 2. Snapshots of several large CMEs from AR 486 during 23 October to 4 November 2003 as observed by SOHO/LASCO. All are LASCO/C2 difference images superposed on EIT difference images, which identify the solar source location, except for the 29 October 2003 halo CME at 2218 UT, which is a LASCO/C3 difference image.

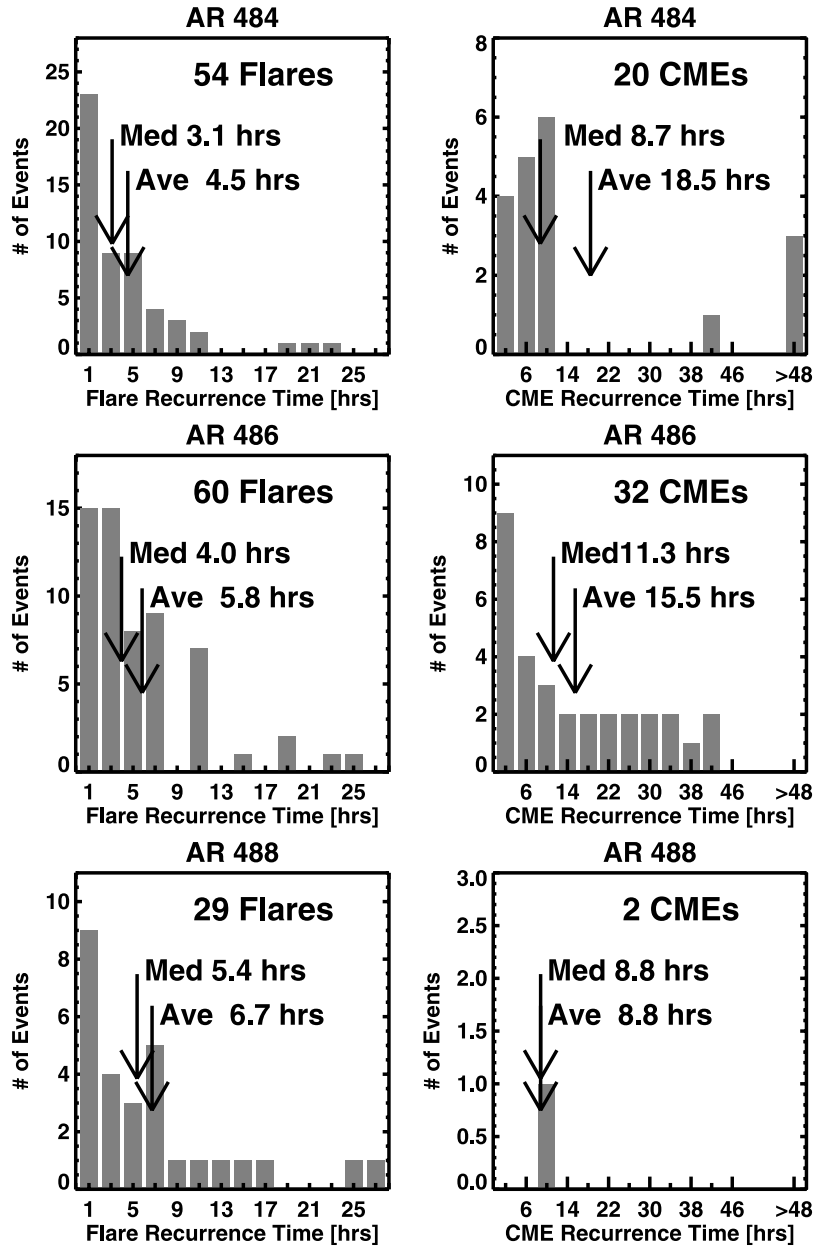

Figure 3. Histograms of flare (left) and CME (right) recurrence times from the three active regions. The total number of flares and CMEs observed from each region, and the average and median recurrence times are also marked. Only two CMEs were identified from AR 488.

made along the position angle (PA) of the fastest feature (PA = 50° for the 28 October CME; PA = 190° for the 29 October CME). AR 484 produced ~20 CMEs, while AR 488 had only two CMEs identified. AR 488 was located very close to AR 486: <30° in latitude and <20° in longitude. It is possible that both regions were involved in some CMEs. Nine CMEs were completely backsided, so the associated active regions are unknown. For seven other CMEs, the source was just behind the limb, but the associated active region could not be identified. Whenever unambiguous, we have listed the associated active region for the behind-the-limb CMEs. When we are less confident about an association, we have added a question mark to the NOAA number or to the heliographic location. Four CMEs were traced to other active regions: two from AR 483 and one each from ARs 491 and 495.

[7] The rapid production of flares and CMEs from the three regions is demonstrated by histograms of recurrence times shown in Figure 3. The recurrence times were obtained as the difference between successive events. The average and median recurrence times are also noted on the plots. The median recurrence time for flares was in the range 3.1–5.4 hours, while it was much higher for CMEs (8.7–11.3 hours). Note that flares and CMEs had recurrence times <4 hours in ARs 484 and 486.

[8] The CME occurrence rate during the October–November interval represents a clear local increase in the solar activity. Figure 4 shows the daily CME rate

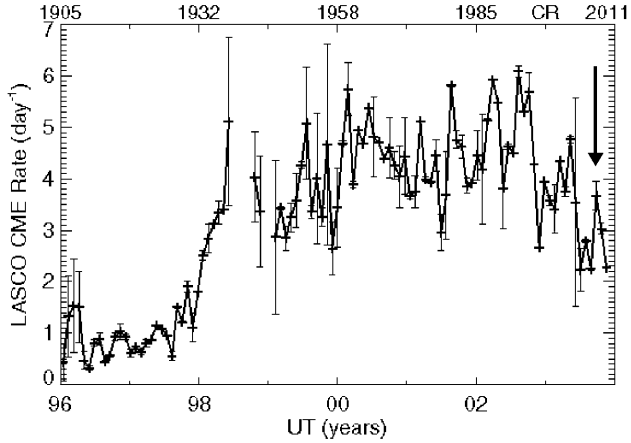

Figure 4. The daily CME rate averaged over Carrington rotation periods from 1996 to the end of 2003. The peak corresponding to the Oct/Nov 03 events is indicated by an arrow. The Carrington Rotation numbers are shown at the top. The error bars were calculated from SOHO downtimes exceeding ~3 hours. The gap in 1998 occurred when SOHO was temporarily disabled for ~3 months in 1998.

averaged over Carrington rotation periods from 1996 to the end of 2003. The CME rate varied from about one every other day during the solar minimum to ~6 per day during the solar maximum phases [*Gopalswamy et al.*, 2003a, 2003b]. Just before the start of the extreme events, the CME rate had fallen to ~2.2 per day. During the storm period, the CME rate increased to ~3.7 per day, representing an increase of ~68%. It must be pointed out that such local activity maxima are not uncommon: A dozen such spikes can be seen in Figure 4, corresponding to the disk passage of some ARs with copious production of CMEs. There was an even bigger spike in 2004 (not shown).

4.1. CME Speeds

[9] The distribution of the Oct/Nov 03 CME speeds is shown in Figure 5. For comparison, we have also shown the distribution of speeds of all the CMEs observed from the beginning of 1996 to the end of 2003 from *Gopalswamy* [2005d]. In the general population, there were 8016 CMEs identified over the 8-year period, but it was possible to measure the speeds of only 7586 CMEs (see *Gopalswamy et al.* [2003b] and *Yashiro et al.* [2004]

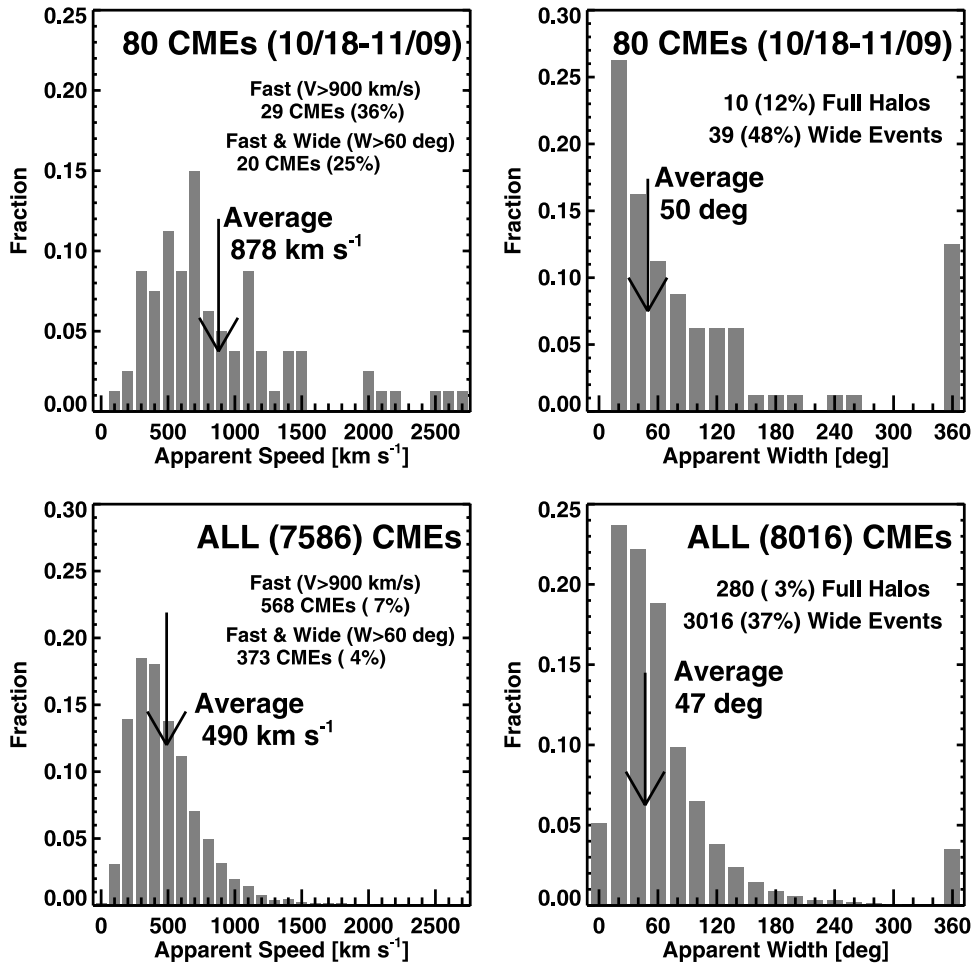

Figure 5. (top) Distribution of CME speeds and widths compared with (bottom) corresponding distributions of the general population. The fraction of fast CMEs, wide CMEs, fast and wide CMEs, and full-halo CMEs in each distribution is shown on the plots. The average values of the distributions are also shown.

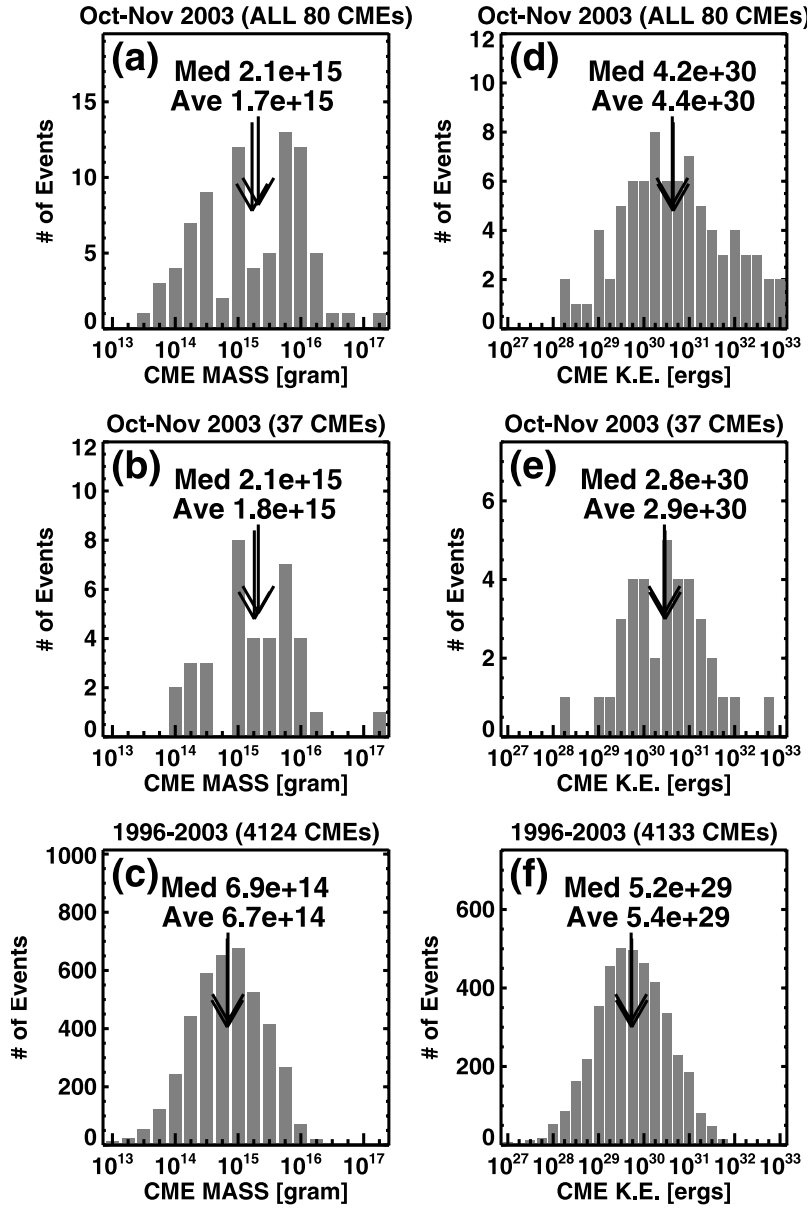

Figure 6. Distribution of (left) mass and (right) kinetic energy of the Oct/Nov 03 CMEs in comparison with those of the general population (1996–2003, inclusive). From the general population (bottom panels), we excluded full halos, 14 small CMEs with masses less than 10^{13} g, and CMEs with less than four height-time measurement points. The histograms in the middle panels were obtained with the same criterion on the number of height-time measurements. The histograms in the top panels were made by including all the 80 mass measurements. The median values of the distributions are marked.

for details). While the range of speeds of the Oct/Nov 03 CMEs is similar to that of the general population, the details are different. The average speed of the 2003 Oct/Nov 03 CMEs was 878 km s^{-1}, considerably larger than that of the general population (490 km s^{-1}). Seven of the 80 CMEs (or 9%) had speeds exceeding 2000 km s^{-1}, while only 25 of the general population (0.3%) were that fast, i.e., more than one-fourth of the superfast events over cycle 23 occurred during the 3-week period of extreme events. On the basis of IP type II burst association, *Gopalswamy et al.* [2001b] had designated CMEs with speeds $\geq$900 km s^{-1} as fast CMEs. More than a third (29/80) of Oct/Nov 03 CMEs were fast events, whereas only 7% of the general population had speeds $\geq$900 km s^{-1}.

4.2. CME Widths

[10] The apparent angular widths of the of the Oct/Nov 03 CMEs are also shown in Figure 5 in comparison with those of the general population. The last bins of the width distributions show the full-halo CMEs (apparent width = 360°). The full halo CMEs appear to surround the occulting disk of the coronagraph [*Howard et al.*, 1982]. Clearly, the Oct/Nov 03 CMEs contained a large fraction (12%) of full halo CMEs compared with the general population (3%). Excluding CMEs wider than 120°, we found similar widths

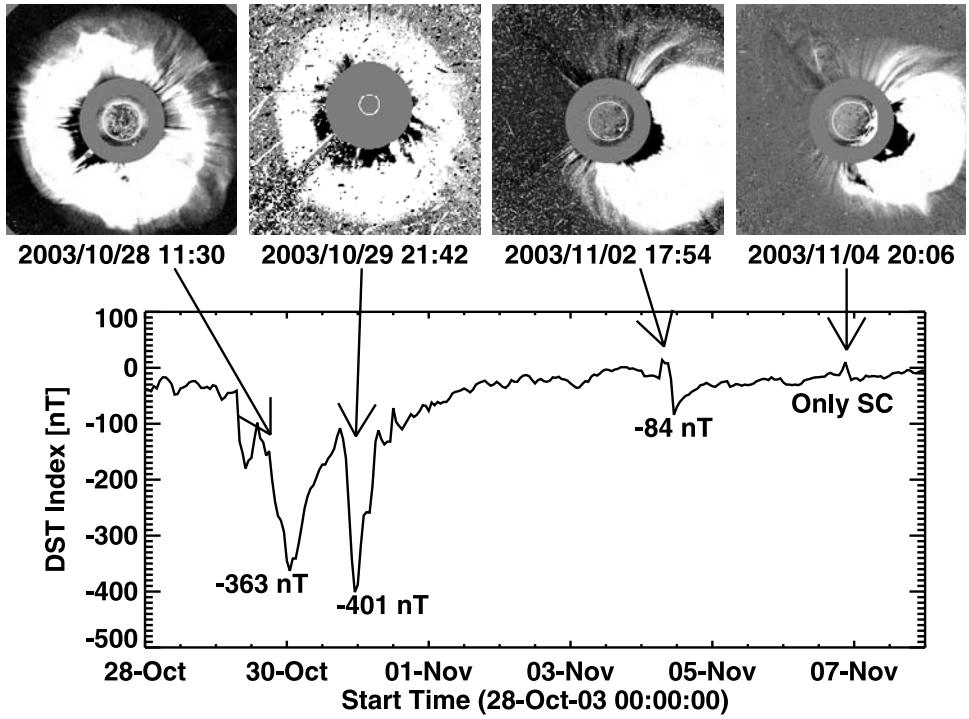

Figure 7. Plot of the Dst index from 26 October to 6 November showing the three intervals of intense geomagnetic storms and several sudden impulses caused by shock impact. The two largest storms are associated with the full halo CMEs on 28 October at 1106 UT from S16E08 and 29 October at 2021 UT from S15W02 as pointed by arrows. The 4 November CME was the fastest in the study period, but was moving orthogonal to the Sun-Earth line, so resulted in just the shock impact at Earth as a sudden impulse. The first dip on 29 October (−180 nT) was after the arrival of the shock from the 28 October, 1106 UT CME, but before the arrival of the IP CME.

for the general population (W = 47°) and the Oct/Nov 03 CMEs (W = 50°). If we consider only wide CMEs (W $\geq$ 60°), the Oct/Nov 03 population has a slightly larger fraction (48%) compared with the general population (37%). Fast and wide CMEs constitute a special population that has significant heliospheric consequences because they often drive shocks (that accelerate electrons and ions) and produce geomagnetic storms [*Gopalswamy et al.*, 2003c]. The abundance of fast and wide CMEs during the Oct/Nov 03 period resulted in a large number of type II radio bursts in the corona and IP medium (see section 5.1). The mass of CMEs is proportional to their apparent width, which implies that the Oct/Nov 03 CMEs, on the average, were very energetic.

4.3. CME Mass and Kinetic Energy

[11] We need to estimate the volume of a CME and the number of electrons contained in it in order to determine its mass. Coronagraph observations can be used to get these estimates if we make some assumptions on the line of sight depth of the CME and the composition of the CME plasma (fully ionized hydrogen plasma with 10% helium [see, e.g., *Vourlidas et al.*, 2002]). Table 1 lists the masses of the 80 CMEs determined in this way. Figure 6 compares the mass distribution of the Oct/Nov 03 CMEs (Figures 6a and 6b) with that of the general population (Figure 6c). Full halo CMEs were excluded from the general population because the error in mass estimates for these CMEs is generally very large. We also excluded those CMEs with fewer than six height-time measurements because the mass values generally change up to a height of ~8 Rs before reaching a constant value [*Vourlidas et al.*, 2002; *Gopalswamy*, 2005d]. We also excluded 14 CMEs with masses $<10^{13}$ g from the general population. The average mass for the general population (6.9×10^{14} g) is lower than those from pre-SOHO observations because SOHO/LASCO can detect a lot of weak CMEs (mass $<10^{14}$ g) owing to its high sensitivity and dynamic range [*Gopalswamy*, 2005d]. Only 37 CMEs from the Oct/Nov 03 time period satisfied the criteria applied to the general population. The mass distribution of the 37 CMEs is shown in Figure 6c, which has a median (average) value of 2.3×10^{15} g (1.8×10^{15} g). This is about 3.3 times larger than the median mass of the general population. If we use all the 80 CMEs, the median and average values did not change significantly. It must be pointed out that the mass we determined is the excess mass (the preevent coronal background has been subtracted), so the mass estimate is a lower limit. From the mass and speed, we obtained the kinetic energy of the CMEs, also shown in the right hand columns of Figure 6. The average and median kinetic energies of the Oct/Nov 03 CMEs were nearly an order of magnitude higher than the corresponding values for the general population.

[12] From Table 1 we can see that 13 CMEs had kinetic energies exceeding 10^{32} erg: 10 from AR 486 (CME 14, 27, 38, 52–54, 64, 71, 77, 78), two from AR 484 (CME 41, 63) and one from AR 488 (CME 66). The 2003 October 28

Table 2. Shocks Near the Sun and at Earth Inferred From Radio and In Situ Observations

	CME			Flare				Metric		DH		Earth		
Number	Date/Time	V	W	Time	Class	Location	NOAA	Time	Freq.	Time	Freq.	Date/Time	Dst, nT	T, hours
9	2003/10/19 0654	798	38	0608	M1.9	N07E65	484	—	—	0715	5000–2000	—	—	—
11	2003/10/19 1708	472	150	1629	X1.1	N06E61	484	1654	030–180	—	—	—	—	—
14	2003/10/21 0354	1484	360	—	—	SE90b	486-	0347	040–110	0410	5000–1000	10/24 1447	−23	60.7
21	2003/10/22 0830	719	267	—	—	N07E25?	484?	0948	025–043	—	—	—	—	—
27	2003/10/23 0854	1406	236	0819	X5.4	S18E88	486	0827	033–109	—	—	10/26 0749	−72	82.7
29	2003/10/23 2006	1136	95	1950	X1.1	S17E88	486	—	—	—	—	10/26 1835	−72	70.5
–	2003/10/24 1106?	365	33	1031	C9.1	N04W02	484	1047	040–065[a]	—	—	—	—	—
34	2003/10/25 0518	685	113	0417	M1.2	S14E45	486	0427	030–050	—	—	—	—	—
–	2003/10/25 0630?	—	—	0544	M1.7	S12E49	486	0552	025–180	—	—	—	—	—
38	2003/10/26 0654	1371	207	0557	X1.2	S15E43	486	0616	057–330	0700	8000–1500	—	—	—
41	2003/10/26 1754	1537	171	1721	X1.2	N04W43	484	1735	030–070	1745	14000–1500	10/28 0130	−42	31.8
52	2003/10/28 1130	2459	360	1100	X17.	S20E02	486	1102	025–180	1110	14000–40	10/29 0600	−363	18.9
54	2003/10/29 2054	2029	360	2037	X10.	S19W09	486	2042	060–430	2055	11000–500	10/30 1620	−401	19.7
62	2003/11/01 2306	899	93	2226	M3.2	S12W60	486	2234	033–180	2255	14000–2000	—	—	—
63	2003/11/02 0930	2036	360	—	—	Backside	—	0916	040–085	0923	14000–630	—	—	—
64	2003/11/02 1730	2598	360	1703	X8.3	S18W59	486	1714	025–180	1730	12000–250	11/04 0553	−68	36.8
65	2003/11/03 0159	827	65	0109	X2.7	N08W73	488	0124	025–180	0115	3000–1500	—	—	—
66	2003/11/03 1006	1420	103	0943	X3.9	N08W78	488	0951	025–180	1000	6000–400	—	—	—
71	2003/11/04 1954	2657	360	1929	X28.	S18W88	486	2003	020–090	2000[b]	10000–200	11/06 1856	−27	47.2

CME (52) had the largest kinetic energy (1.2×10^{33} erg), while a backside CME (63 on 2 November 2003 at 0930 UT) from AR 484 had the second largest kinetic energy (9.3×10^{32} erg). The fastest CME of the study period, also from AR 486 (4 November 2003 at 1954 UT) had comparable kinetic energy (6.1×10^{32} erg). Thus AR 486 stands out as the region producing the largest number of energetic CMEs. We shall return to a discussion on the implication of the high kinetic energies in section 7.

5. Shock Associations

[13] Solar radio bursts of type II are indicative of fast mode MHD shocks in the corona and IP medium. This rare phenomenon involves several processes such as shock formation, particle acceleration, and radiation generation by nonthermal electrons. The radio emission occurs as a result of plasma processes involving low-energy (~10 keV) electrons accelerated at the shock front. The close association of type II bursts and CMEs is thought to be an indication that CMEs drive the shocks by virtue of their super-Alfvenic motion in the corona and IP medium (see *Gopalswamy* [2004a] and *Cliver et al.* [2004b] for a review). Some of these shocks survive to large distances in the heliosphere and are detected in situ by spacecraft instruments. Shocks propagating even orthogonal to the Sun-Earth line can be detected via their type II radio emission, so the number of shocks near the Sun is typically larger than the number detected at Earth. In some cases, flanks of IP shocks driven by limb CMEs are encountered at Earth. Table 2 compiles 19 shocks inferred from type II radio bursts (metric or decameter-hectometric (DH)) and/or from in situ observations. Most of these shocks were identified from the Proton Monitor on board SOHO. In addition to the properties of associated CMEs such as speed (V) and width (W), information on the associated flares is also given. Note that all the 11 X-class flares during the Oct/Nov 03 period are associated with one or other of the shock events in Table 2. Two CMEs in Table 2 do not have an assigned number in Table 1 because they were not listed in the catalog. The CME on 24 October 2003 at 1106 was very faint and was associated with a C9.1 flare from N04W02. The 25 October 2003 event seems to have occurred immediately after the previous event, so it was not possible to measure it.

5.1. Shocks Near the Sun

[14] Type II bursts at metric and DH wavelengths are indicative of shocks near the Sun from 0.5 to a few Rs from the solar surface. Since the conditions for the formation of shocks at metric wavelengths are less stringent [*Gopalswamy et al.*, 2001a], metric type II bursts are more abundant than the DH type II bursts. For the Oct/Nov 03 period, 17 metric type II bursts were reported by the SGD, 11 of which were associated with DH type II bursts. This is a relatively high ratio (69%) compared with 36–38% for the 1996–2002 period [*Gopalswamy et al.*, 2004a; *Cliver et al.*, 2004a]. Two additional DH bursts occurred without metric counterparts. One was a backside event and the other was a CME interaction signature [*Gopalswamy et al.*, 2001d] related to the 4 November 2003 CME. Only 12% (17/143) of the flares and 21% (17/80) of the CMEs were associated with metric type II bursts. The association rate rapidly increased with flare size: 1% (1/87) of C-class, 9% (3/45) of M-class, and 91% (10/11) of the X-class flares were associated with metric type II bursts. Interestingly, one of the X-class flares (23 October 2003) lacked both metric and DH type II bursts. Another X-class flare on the same day (X5.4 flare at 0849 UT) had a metric type II burst but no DH type II burst. The DH type II bursts indicate that the underlying shocks have left the outer corona and are likely to survive for long distances. Six of the 12 DH type II bursts had associated emission from metric to kilometric wavelengths; CMEs associated with these type II bursts are known to be the most energetic.

5.2. Shocks Near Earth

[15] Table 2 shows that all but one of the shocks detected in situ were associated with X-class flares and type II bursts (metric and DH). The single exception was the shock on

Table 3. Historical Fast Transit Shocks Compared With Those of the October–November 2003 Period

Number	Flare Date	UT	Location	Area	SC Date	SC UT	T	V_{inf}	Ref.[h]
01	1 Sep 1859	1118	N20W12	2300	2 Sep	0448	17.5	2356	N
02	15 Jul 1892	1700	S31E32	829	16 Jul	1230[e]	19.5	2144	H,N
03	10 Sep 1908	0536	S21W22	494	11 Sep	0947	28.2	1605	H
04	24 Sep 1909	1006	S05W08	605	25 Sep	1143	25.6	1728	H,N
05	10 Nov 1916	1542	N24E18[c]	142	11 Nov	1912	27.5	1636	N
06	14 Feb 1917	1606	S23E44[c]	110	15 Feb	1200	19.9	2108	N
07	25 Jan 1926	2000	N21W17	3285	26 Jan	1648[f]	20.8	2033	N
08	31 Jul 1937	1642	N24E67[d]	634	1 Aug	2136	28.9	1575	N
09	16 Jan 1938	0040	N17E31	3179	16 Jan	2235	21.8	1958	CS,N,Ca
10	15 Apr 1938	0830	N27W12	1098	16 Apr	0542	21.2	2002	Cb
11	28 Feb 1941	0930[a]	N12W14	683	1 Mar	0354	18.4	2253	CS,Ca,N1
12	17 Sep 1941	0836	N11W09	1896	18 Sep	0448	19.8	2117	N,CS,Ca
13	28 Feb 1942	1242	N07E03	1865	1 Mar	0812	19.5	2144	N, Ca
14	6 Feb 1946	1628	N27W19	4799	7 Feb	1018	17.8	2320	Ca,Cb
15	25 Jul 1946	1504	N21E16	4279	26 Jul	1842	27.6	1631	Cb,NGDC
16	20 Jan 1957	1100	S30W18	557	21 Jan	1254	25.9	1712	Cb,NGDC
17	9 Feb 1958	2108	S12w14	756	11 Feb	0124	28.3	1600	Cb,NGDC
18	10 May 1959	2102	N18E47	1552	11 May	2324	26.4	1688	Cb,NGDC
19	14 Jul 1959	0325	N17E04	1314	15 Jul	0800	28.6	1587	Cb,NGDC
20	16 Jul 1959	2114	N16W31	1981	17 Jul	1642	19.5	2144	Cb,NGDC
21	12 Nov 1960	1315	N28W01	1740	13 Nov	1023	21.2	2002	CS,Ca,E
22	4 Aug 1972	0620	N04E08	1140	4 Aug	2054	14.6	2847	Ca,Cb
23	14 Jul 2000	1024[b]	N22W07	490	15 Jul	1417	27.9	1670[g]	G,NGDC
24	26 Oct 2003	1741[b]	N04W43	1420	28 Oct	0130	31.8	1537[g]	T,NGDC
25	28 Oct 2003	1106[b]	S20E02	2110	29 Oct	0600	18.9	2459[g]	T,NGDC
26	29 Oct 2003	2041[b]	S19W09	2680	30 Oct	1620	19.7	2029[g]	T,NGDC

[a]Based on a crochet in the Abinger magnetic traces [*Newton*, 1941].
[b]Time of CME onset at 1 Rs.
[c]The area of the associated active regions is rather small, so the level of confidence on the flare associations is low.
[d]The flare longitude makes the association questionable, although one cannot rule out intense storms from off-center CMEs [see, e.g., *Gopalswamy*, 2002].
[e]*Hale* [1931] gives a second more violent storm at 1730 UT, which would have resulted in a longer transit time (24.5 hours) and hence a smaller inferred CME speed (1788 km/s).
[f]*Newton* [1943] gives the transit time as 24 hours, even though the difference between the listed flare and geomagnetic storm onsets is only 20.8 hours.
[g]Events 23–26 are from the SOHO era, where 23 is the Bastille Day event and 24–26 are from Table 1.
[h]Ca is *Cliver et al.* [1990a]; Cb is *Cliver et al.* [1990b]; CS is *Cliver and Svalgaard* [2004]; E is *Ellison et al.* [1961]; G is *Gopalswamy et al.* [2005b]; H is *Hale* [1931]; N is *Newton* [1943]; N1 is *Newton* [1941]; NGDC is National Geophysical Data Center for active region area (Greenwich for 1946–1959 and USAF_MWL for 2000–2003) from ftp://ftp.ngdc.noaa.gov/STP/SOLAR_DATA/SUNSPOT_REGIONS/; T is Table 1.

24 October at 1447 UT, tentatively associated with a fast CME (14 in Table 1) originating from behind the east limb on 21 October at 0354 UT from AR 486. It is likely that the associated flare was occulted. However, there was another candidate fast (1085 km s^{-1}) CME (24) from AR 486 (S17E88) associated with an M9.9 flare. The shock on 26 October at 0749 UT was associated with an X5.4 flare but had only a metric type II burst. It must be pointed out that that the Wind spacecraft was located in the tail region of Earth's magnetosphere during the October period, so the background noise was high, which prevented the detection of type II radio bursts below ~1 MHz. The Sun-Earth shock travel times ranged from 18.9 hours (associated with the 28 October CME at 1130 UT) to 82.7 hours (associated with the 23 October CME at 0824 UT). Three of the shocks were associated with CMEs originating from close to the disk center (26 October (1754 UT), 28 October (1130 UT), and 29 October (2054 UT) all from AR 486). At 1 AU, these shocks continued to be driven by the IP counterparts of CMEs [see *Skoug et al.*, 2004; *Tokumaru et al.*, 2005].

[16] The Dst indices of the geomagnetic storms that followed the shocks are also given in Table 2. Shocks associated with CMEs originating far from the disk center did not result in significant geomagnetic storms because the associated IP CME does not reach Earth. Any weak storms following these shocks are likely to be due to the sheath region. The two shocks associated with CMEs originating from close to the disk center were followed by intense geomagnetic storms with Dst = −363 nT on 29 October and −401 nT on 30 October. It must be noted that the two most intense storms were among the top five storms of solar cycle 23. The largest storm of the cycle was on 20 November 2003 (Dst = −472 nT) due to a CME from AR 501 on 18 November 2003. AR 501 was the return of AR 484. The circumstances that enabled this CME to produce the largest storm of the cycle have been reported elsewhere [*Gopalswamy et al.*, 2005a].

5.3. Shock Travel Time Comparison

[17] We now compare the arrival times of the three shocks followed by ICMEs with those of the historical events. Table 3 shows a list of shocks that had a Sun-Earth travel time (T) ≤30 hours, compiled from published literature [*Cliver et al.*, 1990a, 1990b; *Cliver and Svalgaard*, 2004; *Hale*, 1931; *Newton*, 1943]. This list is fairly exhaustive and were based on flare and geomagnetic storm observations. The shock arrival time for the events from before the space era is assumed to be the time of sudden commencement (SC) of geomagnetic storms. *Hale* [1931] published a list of events for the period up to 1930. *Newton* [1943] extended this list by adding events up to the

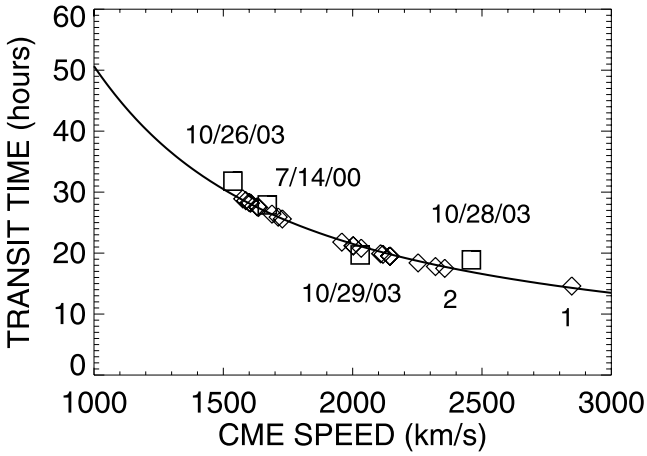

Figure 8. The empirical CME arrival (ESA) model curve ($T = ab^V + c$ with a = 151.002, b = 0.998625, and c = 11.5981) with the travel times of historical events. The diamond symbols represent pre-SOHO historical events with shock transit times from Table 3 and CME speeds inferred from the ESA model. For the three 2003 October events (10/26/03, 10/28/03, 10/29/03) and the Bastille Day event (07/14/00), the data points (squares) are from actual measurements of CME speeds and shock travel times (as listed in Table 3). The two fastest historical events are also indicated as 1 (4 August 1972) and 2 (1 September 1859).

beginning of 1942. *Cliver et al.* [1990a, 1990b] considered events in the period 1938–1989 that might be expected to have high flow velocities at Earth. *Cliver and Svalgaard* [2004] considered fast transit events (Sun-Earth travel time $\leq$21.8 hours) for the period 1859–2003. The SOHO mission started producing CME data from the beginning of 1996. There were no fast transit events during the SOHO epoch other than the ones listed in Table 3 [*Manoharan et al.*, 2004; *Gopalswamy et al.*, 2005d]. We also searched in the catalog of shocks detected at L1 by the Proton Monitor of the Charge, Element, and Isotope Analysis System (CELIAS) on board SOHO. We did not find any shock with a Sun-Earth travel time $\leq$30 hours until March 2005. The 14 July 2000 eruption (the so-called Bastille Day 2000) event was considered in several papers [see, e.g., *Lepping et al.*, 2001]. The Bastille Day shock had a Sun-Earth travel time of 27.8 hours. The 26 October 2003 CME had a shock that is not strictly a fast transit event (T = 31.8 hours) but is shown here because of it almost made the list. We did not have other data sources to check for events with transit time in the range 22–30 hours for the period 1989–1996. For pre-SOHO events, the Sun-Earth travel times of the shocks were obtained as the time elapsed since the flare onset (columns 2–3) to the storm sudden commencement (columns 6–7). The transit times of the SOHO-era shocks were obtained as the difference between CME onset at 1 Rs and the shock arrival time at SOHO (located at the Sun-Earth L1 point). As the time difference between flare onset and CME onset is very small for the fast CME events, we think this transit time is close to the actual transit time. The average transit time of the events listed in coulmn 8 is $\sim$22.95 hours.

[18] The heliographic coordinates of the solar eruption as obtained from the location of the associated flare is given in cloumn 4 of Table 3. It is well known that the Earth-impacting solar events typically originate from close (CMD <30°) to the disk center [see, e.g., *Newton*, 1943; *Cliver et al.*, 1990a], much before the discovery of CMEs. The events listed in Table 3 generally follow this rule, except for the 31 July 1937 event, originating from E67. The shock transit time for this event is among the highest (T = 28.9 hours), so it is possible that the nose speed of the eruption was even higher. We have also listed (in column 5) the active region areas (in units of millionths of solar hemisphere (msh)) compiled from the published literature, when available or from the online archives at the National Geophysical Data Center (NGDC) (ftp://ftp.ngdc.noaa.gov/STP/SOLAR_DATA/SUNSPOT_REGIONS/). The active region areas generally large, except for two events (5 and 6 in Table 3).

[19] All of the pre-SOHO historical events belong to an era preceding the discovery of white light CMEs, so they cannot be directly compared with the Oct/Nov 03 events. However, we can infer the CME speeds for these events based on the empirical shock arrival (ESA) model [*Gopalswamy et al.*, 2003d, 2005d]. The ESA model predicts the travel time of CME-driven shocks taking the CME speed near the Sun as input. The model was an extension of the empirical CME arrival model [*Gopalswamy et al.*, 2001c] based on the shock standoff distance from the driving CME, implied by gas dynamics. The ESA model can be conveniently approximated by the functional form,

$$T = a\,b^V + c; a = 151.002, b = 0.998625, c = 11.5981. \quad (1)$$

Here T is the travel time from CME onset at the Sun to the shock arrival at 1 AU and V is the average CME speed near the Sun (average speed within the coronagraphic field of view). This model predicts a shock travel time of $\sim$13.5 hours to Earth for a CME leaving the Sun center at a speed of 3000 km s^{-1}. A CME has to have a near-Sun speed of $\sim$4300 km s^{-1} for its shock to arrive at 1 AU in 12 hours. An important implication is that we always have a warning of at least 0.5 days for space weather effects if this model is correct. Equation (1) is a good approximation to the ESA model for speeds exceeding $\sim$400 km s^{-1}. For smaller speeds, one has to use the actual model [*Gopalswamy et al.*, 2005d]. Column 9 of Table 3 gives the near-Sun CME speed (V_{inf}) for the historical events, as inferred from equation (1). Not surprisingly, all the inferred speeds exceed 1500 km s^{-1}, while the average speed of the historical events is $\sim$1957 km s^{-1}. Note that this speed is larger than the average speed of CMEs associated with SEP events (1446 km s^{-1}) and with type II radio bursts with counterparts in all wavelength domains (1490 km s^{-1}) [*Gopalswamy et al.*, 2005c].

[20] In Figure 8 we have plotted the ESA model for speeds exceeding 1000 km s^{-1} because we are considering very energetic events. The historical events are shown by the diamond symbols. Remember that the historical events are located on the ESA model curve because the speeds were inferred from the curve itself. The SOHO events, shown by square symbols, clearly overlap with the historical events. The SOHO data points were obtained from independent measurements, so the agreement with the

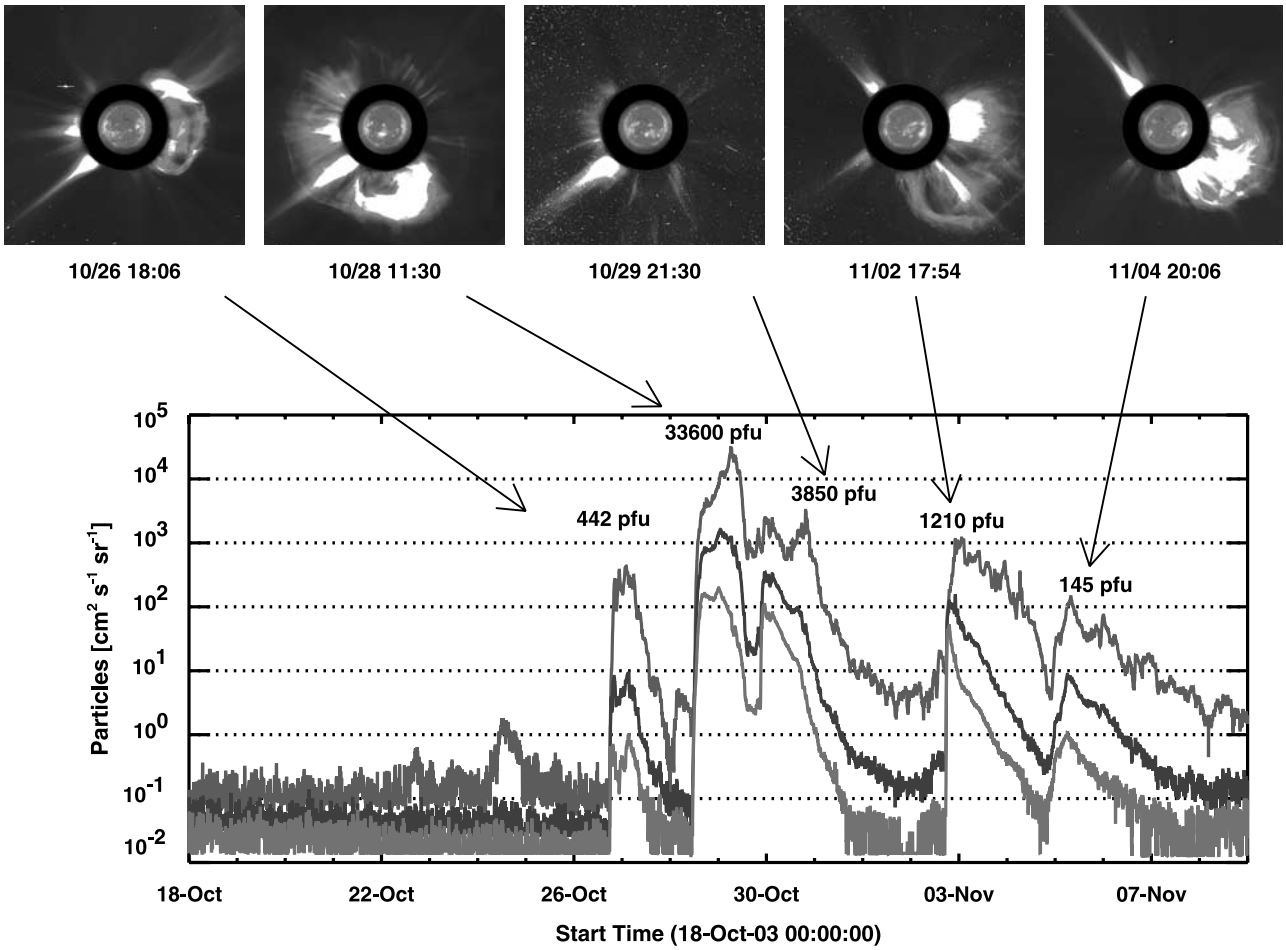

Figure 9. GOES proton intensity from 18 October 18 to 9 November 2003 showing several large SEP events. The peak values of the SEP intensity in the >10 MeV channel are indicated on the plots. The three plots represent the three energy channels: >10 MeV (red), >50 MeV (blue), and >100 MeV (green). The corresponding SOHO/LASCO CMEs are also shown. The bright compact regions in the SOHO/EIT images are the flaring regions. There is also another SEP event on 2 November at 1100 UT before the 1570 pfu event. See color version of this figure at back of this issue.

model is rather good. The two halo CMEs from October 2003 clearly belong to the class of historical extreme events. The 28 October 2003 event (T = 18.9 hours) is very close to the Carrington event (T = 17.5 hours) in terms of the shock travel time. There were only four other events with shorter transit times: 28 February 1941 (T = 18.4 hours), 28 February 1942 (T = 18.5 hours), 6 February 1946 (T = 17.8 hours), and 4 August 1972 (T = 14.5 hours). One can infer a CME speed of ~2847 km s^{-1} for the 4 August 1972 event (the fastest event in Table 3, with T = 14.6 hours). The 4 November 2003 CME came very close to it (speed ~2670 km s^{-1}). This was the fastest CME during the Oct/Nov 03 period. The CME occurred very close to the limb, so the measured speed is likely to be close to the true speed. Only the eastern flank of the shock driven by this CME arrived at Earth after about 47 hours, so the CME is not shown in Figure 8. If it had been Earth-directed, the associated shock would have arrived in a matter of ~15 hours. There were two occasions after the Oct/Nov 03 period, when the near-Sun CME speed was higher: the 10 November 2004 CME at 0226 (from N09W49) had a speed of 3387 km s^{-1}, and the 15 January 2005 CME at 2306 UT (from N15W05) had a speed of ~2890 km s^{-1}. The Thermal Noise Receiver (TNR) of the WAVES experiment shows a pressure pulse at ~0530 UT and a weak shock at ~1645 UT on 11 November 2004. The shock transit time is >33 hours. For the 15 January 2005 event, the shock arrived at 1 AU at 0715 UT on 17 January (T ~32 hours). Thus both of these CMEs did not result in fast-transit shocks at 1 AU.

6. SEP Association

[21] Shocks associated with fast and wide CMEs are thought to be good accelerators of electrons and ions [see, e.g., *Gopalswamy et al.*, 2003c]. As described above, 18 type II radio bursts were observed over a short interval of 3 weeks indicating the abundance of strong shocks during the Oct/Nov 03 period. In order to see the SEP association of these shocks, we have shown the GOES proton intensity plots for the period 18 October to 9 November 2003 in Figure 9. One can see six large SEP events in the plot. By large SEP event we mean peak intensity ≥10 pfu (1 pfu = 1 proton per (cm^2 s sr)) in the

Table 4. List of SEP Events With Intensity ≥1000 pfu in the >10 MeV Channel

Date/Time	SEP Intensity, pfu	CME Time	AR
1998/04/20 1400	1700	1021	8194
1998/09/30 1520	1200	DG	8340
2000/07/14 1045	24000	1054	9077
2000/11/08 2350	14800	2306	9212[a]
2001/04/02 2340	1110	2200	9393
2001/09/24 1215	12900	1030	9632
2001/10/01 1145	2360	0530	9628
2001/11/04 1705	31700	1635	9684
2001/11/22 2320	18900	2330	9704
2002/04/21 0225	2520	0127	9906
2003/10/28 1215	33600	1130	0486
2003/10/29 2200	3850	2054	0486
2003/11/02 1800	1210	1730	0486

[a]Complex eruption involving two other active regions (AR 9213 and 9218).

>10 MeV channel. After two minor enhancements, the first large SEP event (intensity = 442 pfu) occurred on 26 October in association with the 1754 UT CME from AR 484. The two large halos (28 October at 1130 UT and 29 October at 2054 UT) from AR 486 resulted in the next two large SEP events with intensities of 33600 and 3580 pfu, respectively. There was a brief enhancement of SEP intensity (∼30 pfu) in association with the 0930 UT CME on 2 November (CME 63) from behind the limb. The intensity soon reached a peak value of 1210 pfu during the second event on 2 November at 1730 UT. The last large SEP event (145 pfu) was in association with the 4 November CME at 1954 UT, which was from the west limb. The intensity declined slowly below the 10 pfu level on 7 November and continued to remain above the background level (0.1 pfu) until 18 November, when the return of AR 484 as AR501 started producing SEP-associated CMEs. Figure 9 also shows that there were four intervals during which the SEP intensity in the >10 MeV channel exceeded 1000 pfu, and all of them were associated with CMEs from AR 486. Table 4 lists all the events of solar cycle 23 that had >10 MeV proton intensity exceeding 1000 pfu. There were no high-intensity events in years 1996, 1997, and 1999. Note that all the events were from different active regions, except that all the 2003 events originate in the single region. These three events were also ground level events (GLEs). In cycle 22, AR 5747 produced a similar set of three SEP events during 19–23 October 1989 [see, e.g., *Reeves et al.*, 1992], with the first event having an intensity (≥40,000 pfu) higher than that of the 28 October 2003 event. Another region, AR 5395 during March 1989 produced 11 X-class flares [see *Feynman and Hundhausen*, 1994] with the highest SEP intensity (≥43,000 pfu) recorded since 1976.

7. Active Region Energy

[22] One of the important implications of the results presented in Figure 8 is that the Sun-Earth travel time of CME-driven shocks may not be less than 0.5 day. This result is not only supported by the ESA model prediction but also by the observations of historical extreme events. The high sensitivity and uniform data coverage of SOHO/LASCO has resulted in the detection of more than 8000 CMEs from the launch to the end of 2003. Of these 8000 CMEs, only 25 had speeds exceeding 2000 km s^{-1}. Even among the historical events (Table 3), only 13 had inferred (or measured) speeds exceeding 2000 km s^{-1} and none of them exceeded 3000 km s^{-1}. This suggests that the maximum speed of CMEs may not be too much higher than ∼3000 km s^{-1}. Since CMEs have to be powered by the magnetic free energy built up in active regions, the CME speed limit implies an upper bound to the maximum free energy extractable from the active regions. The free energy in the magnetic fields needs to be estimated from the distribution of currents in the active region corona [see, e.g., *Metcalf et al.*, 1995]. For order of magnitude estimates, one can assume that the free energy is of the order of the energy in the potential field [*Mackay et al.*, 1987; *Metcalf et al.*, 1995; *Forbes*, 2000; *Venkatakrishnan and Ravindra*, 2003]. The energy in the potential field depends on the size and magnetic field strength of the active regions. A good measure of the size of the active region is its area reported in the SGD.

[23] In Figure 10, we have shown the evolution of the areas of the three Oct/Nov 03 active regions. The starting time is when the region first appeared at the east limb and was tracked until it reached the west limb. Clearly, AR 486 had the largest area peaking at 2610 msh and ranks number 1 in cycle 23. The peak values for ARs 484 and 488 were lower (1750 msh) but still were within the top 10 active region areas of solar cycle 23, ranking fifth and sixth largest, respectively. The second, third, and fourth largest active regions were AR 9393 (2240 msh on 29 March 2001), AR 9169 (2140 msh on 20 September 2000), and AR 0069 (1960 msh on 19 August 2002). Figure 10 also shows two other smaller active regions for comparison:

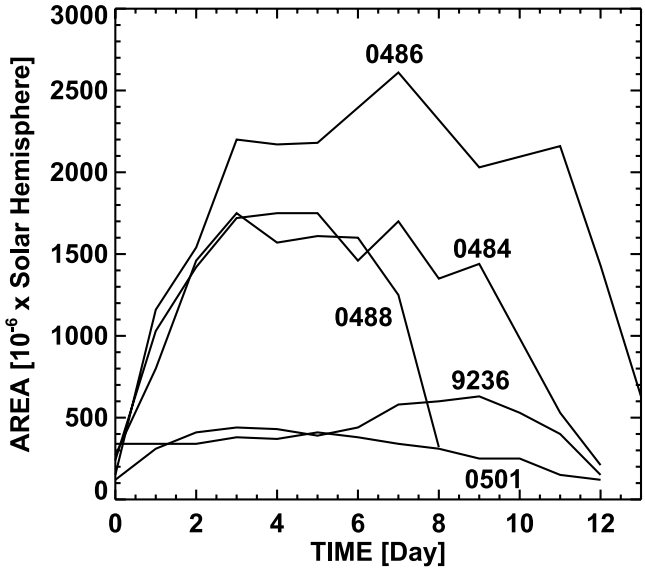

Figure 10. Active region area (millionths of solar hemisphere or msh) for the three active regions, 484, 486, and 488. Two other active regions are also shown for reference: AR 0501 (return of AR 484) and AR9236, which also produced several large eruptions in quick succession during 23–27 November 2000. AR 486 ranked number 1 in solar cycle 23.

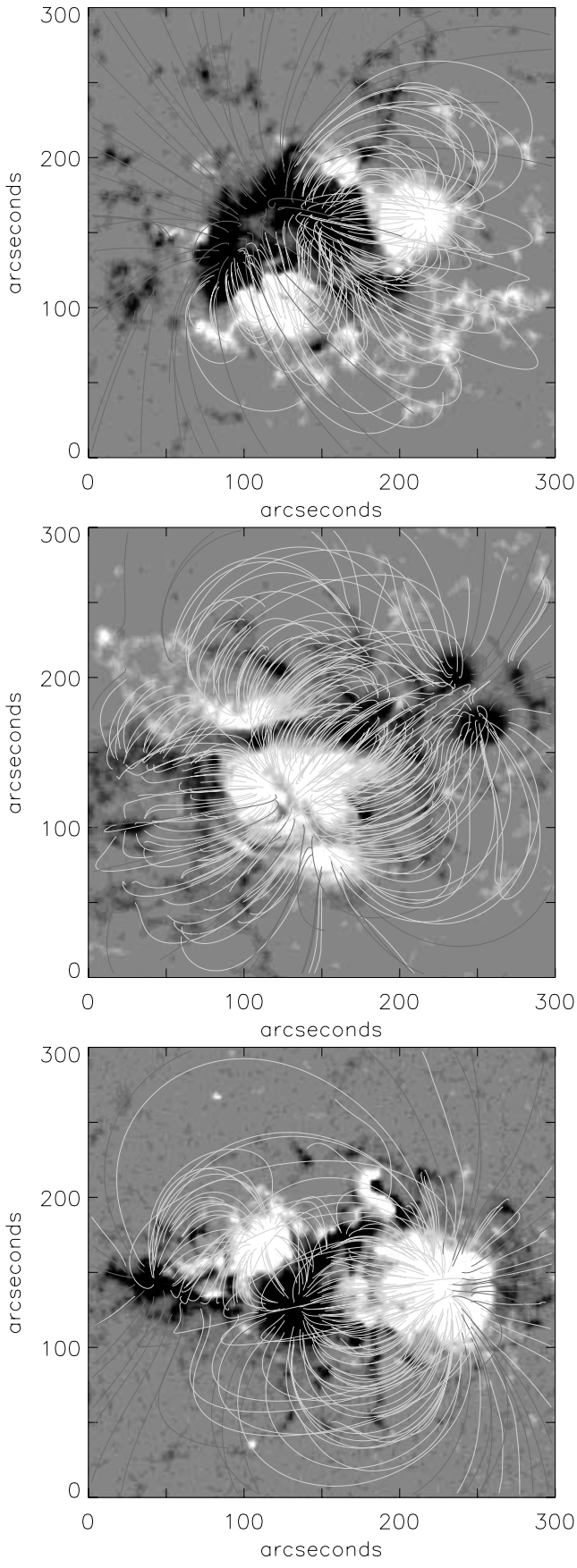

(1) AR 9236 reached a peak value of only 630 msh on 27 November 2000, yet it produced a large number of energetic eruptions [*Gopalswamy et al.*, 2005b]. (2) AR 501 was the return of AR 484 and had a peak area of only 410 msh on 18 November 2003. This region produced CMEs of moderate energy; one of them on 18 November 2003 produced the largest geomagnetic storm of cycle 23 [*Gopalswamy et al.*, 2005a] due to the high inclination of the resulting magnetic cloud. These events provide a cautionary reminder that large geomagnetic storms can originate from unimpressive active regions or even outside of active regions [see also *Dodson and Hedeman*, 1964; *Cliver and Crooker*, 1993; *McAllister et al.*, 1996]. We also note that two of the historical events (5 and 6 in Table 3) had small AR areas (142 and 110 msh). However, one cannot rule out the possibility of misidentification of the associated flares in these cases.

[24] We now estimate the free energy available in the three active regions based on the potential field extrapolation of the photospheric magnetic fields, obtained by SOHO's Michelson Doppler Imager (MDI), assuming that the total energy (free plus potential) of the active region magnetic fields is about twice the potential energy. Under this assumption, the potential energy is a good indicator of the free energy available in the active regions. However, recent calculations suggest that the total energy may be several times the potential energy [*Metcalf et al.*, 2004]. Nevertheless, the potential energy calculated is a useful estimate to compare with the CME kinetic energy.

[25] In Figure 11, we have plotted selected field lines obtained by potential field extrapolation of the SOHO/MDI magnetograms. The potential field was calculated using a Green's Function method [*Chiu and Hilton*, 1977]. The MDI magnetograms were taken at 1911 UT on 23 October for AR 484, 1251 UT on 29 October for AR 486, and 2224 UT on 30 October for AR 488. The volume chosen for an estimate of the potential field energy for each active region is a cube with a side of 300 arcsec. The base of the cube is the area of the panels shown in Figure 11. The MDI data were corrected by a rescaling factor (factor = 1.45) suggested by *Berger and Lites* [2003]. Table 5 shows representative values of the energy of the potential field (Ep) from the three active regions, along with the maximum CME kinetic energy (Max KE) and active region area. Unfortunately, the CME energies and energies of the potential fields could not be estimated for the same events. The main reason is the basic difficulty of making simultaneous mass and magnetic field measurements for all the CMEs: It is easy to measure the magnetic field of disk active regions, but it is difficult to measure the mass of CMEs originating from disk regions; the opposite is true for limb events. Nevertheless, these estimates should suffice for order of magnitude calculations because the potential energy in the field does not change rapidly. The

Figure 11. Selected magnetic field line computed by potential field extrapolation of the SOHO/MDI magnetograms for the three active regions: 484 (top), 486 (middle), and 488 (bottom). Green lines represent closed field lines, while the red shows the field lines running out of the cube. See color version of this figure at back of this issue.

Table 5. Energy Characteristics of the Three Active Regions

AR	Area, msh	Ep, erg	Max KE, erg
AR0484	1750	3.66E+33	2.4e+32
AR0486	2610	4.57E+33	1.2e+33
AR0488	1750	2.76E+33	1.3e+32

magnetic potential energies listed in Table 5 are larger than all the values compiled by *Venkatakrishnan and Ravindra* [2003] for the period 1998–2002. Table 5 shows that the CME kinetic energies reached a significant fraction of the energy of the potential fields (5 to 26% in Table 5). We note that AR 486 stands out as the one with the largest area, containing the largest free energy. The dominance of CME kinetic energy over other forms of energy released during a solar eruption has been reported in case studies [see, e.g., *Webb et al.*, 1980; *Emslie et al.*, 2004]. *Emslie et al.* [2004] estimated that the CME kinetic energy in two SOHO CMEs (21 April 2002 and 23 July 2002) accounts for a substantial fraction of the free energy, although they had to assume the free energy from a similar active region.

7.1. Active Region Area, Flare Size, and CME Speed

[26] In order to compare the areas of the Oct/Nov 03 active regions with those of the other active regions of solar cycle 23, we selected all the regions that had at least one large SEP event during their disk passage. These regions were listed in the work of *Gopalswamy et al.* [2004b] for the period 1996–2002. We added other large SEP events from 2003 to this list, which resulted in 55 events with active region information (from the SGD). As noted before, the time of the SEP event need not fall on the day the associated AR attained its maximum area. It must be pointed out that the set of active regions we have chosen is based on their ability to produce SEP events. The reason for this is that the associated CMEs are expected to be fast and wide, similar to the Oct/Nov 03 CMEs. Figure 12a shows the area distribution of these active regions. Note that the Oct/Nov 03 active regions (AR 486 and 484) belong to the high-area tail of this distribution. Some bins may have multiple counts because the same region produced more than one large SEP event.

[27] Figure 12b shows a scatterplot between the active region area and the size of the flare produced in it. The flares considered are the ones associated with the 55 large SEP events noted above. The X-ray flare size (measured as the peak X-ray intensity in the 1–8 Å band) is reasonably correlated with the active region area (correlation coefficient r = 0.64). We also considered the relation between CME speeds (for the same 55 SEP events) and the corresponding active region areas, but the correlation is much weaker (r = 0.37). It is significant that the Oct/Nov 03 values for all the three quantities (active region area, flare size, and CME speed) occupy the top-right corner of the plots in Figures 12b and 12c). The correlations also suggest that the AR size is a more important determinant of peak flare size than of maximum CME speed. This is understandable because flare loops are confined to the active region, while CMEs expand and occupy a much larger volume after eruption.

[28] The regression line for the flare size (X)-active region area (A) is given by

$$\log X = -8.34 + 1.50 \log A. \quad (2)$$

The CME speed (V) and A are related by

$$\log V = 2.54 + 0.22 \log A. \quad (3)$$

These relations can be used to estimate the flare size of the historical events. For the Carrington flare of 1 September 1859 [*Carrington*, 1860], the size of the sunspot group was estimated by *Hodgson* [1860] as 128 arcsec. From this, the active region area can be estimated as ~2500 msh. A modern estimate of the sunspot area is 2300 msh [*Newton*, 1943]. Substituting this value into equation (2), we get a flare size of X5 for the Carrington flare. From a consideration of the amplitude of the solar flare effect in the Kew/Greenwich magnetograms, *Cliver and Svalgaard* [2004] conservatively concluded that the Carrington flare was ≥X10 soft X-ray event. As for the CME, equation (3) gives a speed of ~1830 km s^{-1}, which is about 22% lower than the speed (2356 km s^{-1}) inferred from the ESA model (equation (1)). Given the weaker correlation of the CME speed with active region area, this agreement is not unreasonable. On the other hand, the 4 August 1972 eruption originated from an active region with an area of only ~1100 msh, yet the associated shock had a mere 14.5 hour transit time. In cycle 23, AR 486 had the maximum area as of this writing. However, AR areas as high as ~5000 msh have been reported for other solar cycles [*Newton*, 1955]. For such a huge region, the flare size expected from equation is ≥X16, which is smaller than the size of the 4 November 2003 flare; the expected CME speed is only ~2260 km s^{-1}. The 6 February 1946 event in Table 3 had the largest area (4799 msh) and one of the fastest events (T = 17.8 hours) with an inferred CME speed of 2320 km s^{-1}. If we substitute A = 4799 in equation (3), we get a CME speed of 2238 km s^{-1}, not too different from the one inferred from equation (1). Thus the correlation between AR area and CME speed is expected to be loose, but a region with large area enhances the probability of occurrence of ultrafast CMEs.

8. Discussion and Conclusions

[29] We studied the violent solar eruptions of 2003 October and November, involving fast CMEs, X-class solar flares, interplanetary shocks, intense geomagnetic storms, and SEPs. These CMEs clearly were shown to be faster and wider (more energetic) on the average than the general population of SOHO CMEs observed over a period of 8 years. The violent solar eruptions of Oct/Nov 03 period can be regarded as extreme events in terms of their origin as well as their heliospheric consequences. At the Sun, the eruptions had a very high recurrence rate. There were many firsts of solar cycle 23 during this period: the largest active region area, the largest X-ray flare, the highest concentration of ultrafast CMEs, the largest SEP event, the fastest IP shock, the highest concentration of IP radio bursts, and the highest solar wind speed [*Skoug et al.*, 2004]. The two Earth-directed full halo CMEs produced intense geomagnetic storms (Dst index of −363 and −401 nT for the 28 and 29 October CMEs, respectively). However, the largest storm of the cycle (Dst = −472 nT) occurred when AR 484 returned as AR 501 and ejected a fully southward magnetic cloud [*Gopalswamy et al.*, 2005a].

[30] Two of the halo CMEs resulted in shocks that arrived at Earth in <24 hours. Historically, there were only 15 such fast-transit events with a Sun-Earth shock travel time of $\leq$1 day. The ESA model curve in Figure 8 suggests that a hypothetical CME with a speed of 3000 km s^{-1} would travel the Sun-Earth distance in about 13.5 hours. The uniform data coverage and high sensitivity CME observations from SOHO have further revealed that the number of CMEs with speeds exceeding 2000 km s^{-1} is exceedingly small: (25/8016 or 0.3%. Only four CMEs had speeds >2500 km s^{-1} (0.05%) over the 8-year period of SOHO operation. Two faster CMEs occurred after the Oct/Nov 03 period and their speeds were also in the vicinity of 3000 km s^{-1} (2861 km s^{-1} on 15 January 2005 and 3387 km s^{-1} on 10 November 2004). The highest CME speed inferred from the ESA model curve for the historical events is 2847 km s^{-1} (4 August 1972 event), also less than 3000 km s^{-1}. From these results, one can infer that CMEs may not have speeds far greater than $\sim$3000 km s^{-1}. This speed limit has a practical implication that CME-driven shocks take at least half a day to reach Earth after their launch at the Sun. In fact the ESA model curve (equation (1)) suggests that a CME has to be launched with a speed of $\sim$4300 km s^{-1} in order for its shock to arrive at 1 AU in $\sim$12 hours. A 0.5-day lead time is very useful for the mitigation of space weather effects related to geomagnetic storms but not for prompt flare effects such as sudden ionospheric disturbances or for SEPs that arrive at Earth in tens of minutes.

[31] The CME speed limit is naturally linked to the amount of free energy available in the active regions. While the actual free energy needs to be computed from vector magnetograms, we used the simpler approach of deriving the potential field energy as a proxy to the free energy. AR 486, which produced all the extreme events, ranked number 1 in terms of active region area and the the potential field energy. The maximum free energy available was a few times 10^{33} erg. The result that up to 26% of the available free energy seems to have gone into the CME kinetic energy makes the CMEs the most energetic phenomena in the interplanetary space. If a larger fraction of the free energy goes into the mass motion or if the active region has even more free energy, then one would expect a faster CME. Historically, active regions much larger than AR 486 have been observed, so we cannot say that events of even greater magnitude may not occur. Nevertheless, an important outcome of this study is an assessment on the magnitude of catastrophic eruptions from the Sun in terms of the maximum free energy available from the Sun. The Oct/Nov 03 episode is the best observed outbreak of solar activity with modern instruments and hence can serve as a benchmark for transient disturbances in the heliosphere. These events also helped us revisit the historical events from the point of view of CMEs and the their interplanetary consequences.

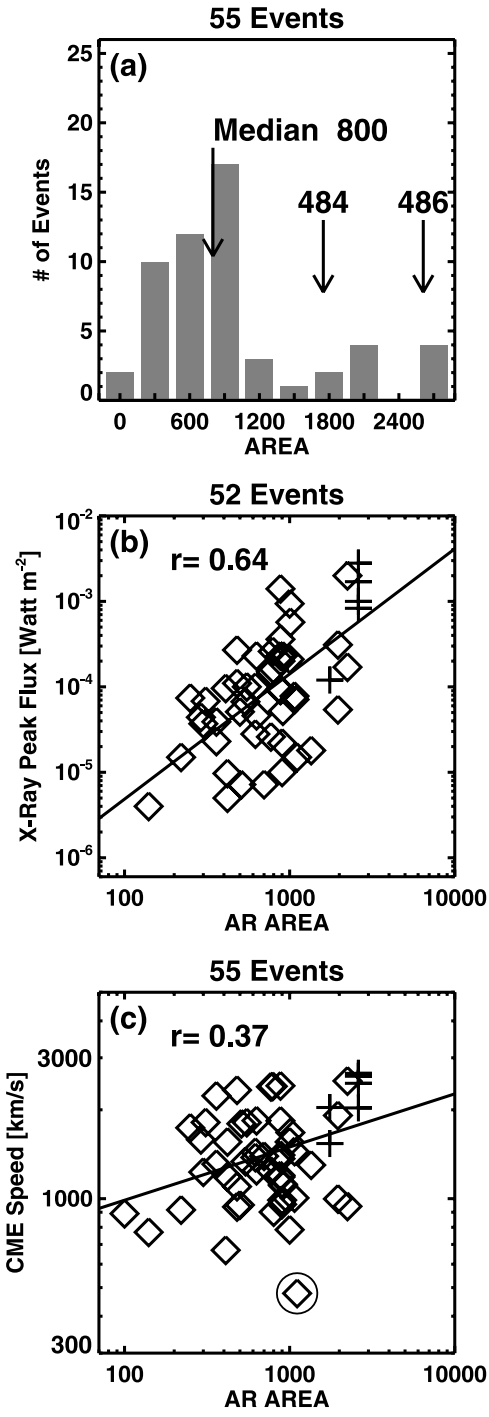

Figure 12. (a) The distribution of areas of active regions that produced at least one large SEP event during its disk passage during solar cycle 23 (1996–2003). The median value of the distribution is 800 msh. Areas of ARs 484 and 486 are indicated by arrows. (b) Scatterplot between GOES X-ray flare size (X) and active region area (A), showing good correlation. Three limb events were excluded because the flare size may be an underestimate due to partial occultation. The flare size is for the SEP events used in Figure 12a. The correlation coefficient, r = 0.64 is shown. The regression line is given by $\log X = -8.34442 + 1.49520 \log A$. (c) Scatter SOHO/LASCO CME speed (V) and active region area (A). The CMEs were associated with the SEP events used in Figure 12a. The correlation is weaker (r = 0.37). The regression line is given by $\log V = 2.53501 + 0.215581 \log A$. One outlier (circled diamond symbol) was not included in determining the correlation coefficient. The Oct/Nov 03 events (plus symbols) clearly lie to the extreme right of the plot.

[32] **Acknowledgments.** The authors thank E. W. Cliver, one of the referees, for helpful comments. Part of this effort was supported by NASA/LWS and NSF/SHINE (ATM 0204588) programs. SOHO is a project of international cooperation between ESA and NASA.

[33] Arthur Richmond thanks E. W. Cliver and Bernard Jackson for their assistance in evaluating this paper.

References

Berger, T. E., and B. W. Lites (2003), Weak-field magnetogram calibration using Advanced Stokes Polarimeter Flux Density Maps - II. SOHO/MDI full-disk mode calibration, *Solar Phys.*, *213*, 213.

Bougeret, J.-L., et al. (1995), Waves: The Radio and Plasma Wave Investigation on the Wind Spacecraft, *Space Sci. Rev.*, *71*, 231.

Brueckner, G. E., et al. (1995), The large angle spectroscopic coronagraph (LASCO), *Solar Phys.*, *162*, 357.

Carrington, R. C. (1860), Description of a singular appearance seen in the Sun on September 1, 1859, *MNRAS*, *20*, 13.

Chiu, Y. T., and H. H. Hilton (1977), Exact Green's function method of solar force-free magnetic-field computations with constant alpha. I - Theory and basic test cases, *Astrophys. J.*, *212*, 873.

Cliver, E. W., and N. U. Crooker (1993), A seasonal dependence for the geoeffectiveness of eruptive solar events, *Solar Phys.*, *145*, 347.

Cliver, E. W., and L. Svalgaard (2004), The 1859 solar-terrestrial disturbance and the current limits of extreme space weather activity, *Solar Phys.*, *224*, 407.

Cliver, E. W., J. Feynman, and H. B. Garrett (1990a), Flare-associated solar wind disturbances with short ($\leq$20 hr) transit times to Earth, in *Solar-Terrestrial Predictions*, vol. 1, edited by R. J. Thompson et al., pp. 348–358, NOAA, Boulder, Colo.

Cliver, E. W., J. Feynman, and H. B. Garrett (1990b), An estimate of the maximum speed of the solar wind, 1938–1989, *J. Geophys. Res.*, *95*, 17,103.

Cliver, E. W., S. W. Kahler, and D. V. Reames (2004a), Coronal shocks and solar energetic proton events, *Astrophys. J.*, *605*, 902.

Cliver, E. W., N. V. Nitta, B. J. Thompson, and J. Zhang (2004b), Coronal shocks of November 1997 revisited: The CME - type II timing problem, *Solar Phys.*, *225*, 105.

Dodson, H. W., and R. E. Hedeman (1964), Problems of differentiation of flares with respect to geophysical effects, *Planet. Space Sci.*, *12*, 393.

Ellison, M. A., S. M. P. McKenna, and J. H. Reid (1961), Flares associated with the 1960 November event and the flare nimbus phenomenon, *MNRAS*, *122*, 491.

Emslie, A. G., et al. (2004), Energy partition in two solar flare/CME events, *J. Geophys. Res.*, *109*, A10104, doi:10.1029/2004JA010571.

Feynman, J., and A. J. Hundhausen (1994), Coronal mass ejections and major solar flares: The great active center of March 1989, *J. Geophys. Res.*, *99*, 8451.

Forbes, T. G. (2000), A review on the genesis of coronal mass ejections, *J. Geophys. Res.*, *105*, 23,153.

Gopalswamy, N. (2002), Relation between CMEs and ICMEs, in *Solar-Terrestrial Magnetic Activity and Space Environment*, *COSPAR Colloq. Ser.*, vol. 14, edited by H. N. Wang and R. L. Xu, p. 157, Springer, New York.

Gopalswamy, N. (2004a), A global picture of CMEs in the inner heliosphere, in *The Sun the Heliosphere As an Integrated System*, edited by G. Poletto and S. Suess, p. 201, chap. 8, Springer, New York.

Gopalswamy, N. (2004b), Recent advances in the long-wavelength radio physics of the Sun, *Planet. Space Sci.*, *52*, 1399.

Gopalswamy, N., A. Lara, M. L. Kaiser, and J.-L. Bougeret (2001a), Near-Sun and near-Earth manifestations of solar eruptions, *J. Geophys. Res.*, *106*, 25,261.

Gopalswamy, N., S. Yashiro, M. L. Kaiser, R. A. Howard, and J.-L. Bougeret (2001b), Characteristics of coronal mass ejections associated with long wavelength type II radio bursts, *J. Geophys. Res.*, *106*, 29,219.

Gopalswamy, N., A. Lara, S. Yashiro, M. L. Kaiser, and R. A. Howard (2001c), Predicting the 1-AU arrival times of coronal mass ejections, *J. Geophys. Res.*, *106*, 29,207.

Gopalswamy, N., S. Yashiro, M. L. Kaiser, R. A. Howard, and J.-L. Bougeret (2001d), Radio signatures of coronal mass ejection interaction: Coronal mass ejection cannibalism?, *Astrophys. J.*, *548*, L91.

Gopalswamy, N., A. Lara, S. Yashiro, S. Nunes, and R. A. Howard, (2003a), Solar variability as an input to the Earth's environment, *ESA SP-535*, p. 403, Eur. Space Agency, Paris.

Gopalswamy, N., A. Lara, S. Yashiro, and R. A. Howard (2003b), Coronal mass ejections and solar polarity reversal, *Astrophys. J.*, *598*, L63.

Gopalswamy, N., S. Yashiro, A. Lara, M. L. Kaiser, B. J. Thompson, P. T. Gallagher, and R. A. Howard (2003c), Large solar energetic particle events of cycle 23: A global view., *Geophys. Res. Lett.*, *30*(12), 8015, doi:10.1029/2002GL016435.

Gopalswamy, N., P. K. Manoharan, and S. Yashiro (2003d), Comment on "Coronal mass ejections, interplanetary ejecta and geomagnetic storms" by H. V. Cane, I. G. Richardson, and O. C. St. Cyr, *Geophys. Res. Lett.*, *30*(24), 2232, doi:10.1029/2003GL017562.

Gopalswamy, N., S. Nunes, S. Yashiro, and R. A. Howard (2004a), Variability of solar eruptions during cycle 23, *Adv. Space Res.*, *34*, 391.

Gopalswamy, N., S. Yashiro, S. Krucker, G. Stenborg, and R. A. Howard (2004b), Intensity variation of large solar energetic particle events associated with coronal mass ejections, *J. Geophys. Res.*, *109*, A12105, doi:10.1029/2004JA010602.

Gopalswamy, N., S. Yashiro, G. Michalek, H. Xie, R. P. Lepping, and R. A. Howard (2005a), Solar source of the largest geomagnetic storm of cycle 23, *Geophys. Res. Lett.*, *32*, L12S09, doi:10.1029/2004GL021639.

Gopalswamy, N., S. Yashiro, S. Krucker, G. Stenborg, and R. A. Howard (2005b), CME interaction and the intensity of solar energetic particle events, in *Coronal and Stellar Mass Ejections, Proceedings of IAU Symposium 226*, edited by K. P. Dere, J. Wang, and Y. Yan, p. 367, Int. Astron. Union, Paris.

Gopalswamy, N., E. Aguilar-Rodriguez, S. Yashiro, S. Nunes, M. L. Kaiser, and R. A. Howard (2005c), Type II radio bursts and energetic solar eruptions, *J. Geophys. Res.*, doi:10.1029/2005JA011158, in press.

Gopalswamy, N., A. Lara, P. K. Manoharan, and R. A. Howard (2005d), An empirical model to predict the 1-AU arrival of interplanetary shocks, *Adv. Space Res.*, in press.

Hale, G. E. (1931), The spectrohelioscope and its work, part III. Solar eruptions and their apparent terrestrial effects, *Astrophys. J.*, *73*, 379.

Hodgson, R. (1860), On a curious appearance seen in the Sun, *MNRAS*, *20*, 15.

Howard, R. A., D. J. Michels, N. R. Sheeley Jr., and M. J. Koomen (1982), The observation of a coronal transient directed at earth, *Astrophys. J.*, *263*, L101.

Lepping, R. P., et al. (2001), The Bastille Day magnetic clouds and upstream shocks: Near-Earth interplanetary observations, *Solar Phys.*, *204*, 285.

Mackay, D. H., V. Gaizauskas, G. J. Rickard, and E. R. Priest (1987), Force-free and potential models of a filament channel in which a filament forms, *Astrophys. J.*, *486*, 534.

Manoharan, P. K., N. Gopalswamy, S. Yashiro, A. Lara, G. Michalek, and R. A. Howard (2004), Influence of coronal mass ejection interaction on propagation of interplanetary shocks, *J. Geophys. Res.*, *109*, A06109, doi:10.1029/2003JA010300.

McAllister, A. H., et al. (1996), A large polar crown coronal mass ejection and a "problem" geomagnetic storm: April 14–23, 1994, *J. Geophys. Res.*, *101*, 13,497.

Metcalf, T. R., L. Jiao, R. C. McClymont, R. C. Canfield, and H. Uitenbroek (1995), Is the solar chromospheric magnetic field force-free?, *Astrophys. J.*, *439*, 474.

Metcalf, T. R., K. D. Leka, and D. L. Mickey (2004), The Magnetic Free Energy in AR 486, paper presented at Meeting 204, Am. Astron. Society, Washington, D. C.

Newton, H. W. (1941), The great magnetic storm of 1941, March 1, *Observatory*, *64*, 82.

Newton, H. W. (1943), Solar flares and magnetic storms, *MNRAS*, *103*, 244.

Newton, H. W. (1955), The lineage of the great sunspots, *Vistas Astron.*, *1*, 666.

Reeves, G. D., T. E. Cayton, S. P. Gary, and R. D. Belian (1992), The great solar energetic particle events of 1989 observed from geosynchronous orbit, *J. Geophys. Res.*, *97*, 6219.

Skoug, R. M., J. T. Gosling, J. T. Steinberg, D. J. McComas, C. W. Smith, N. F. Ness, Q. Hu, and L. F. Burlaga (2004), Extremely high speed solar wind: 29–30 October 2003, *J. Geophys. Res.*, *109*, A09102, doi:10.1029/2004JA010494.

Tokumaru, M., M. Kojima, K. Fujiki, M. Yamashita, and D. Baba (2005), Interplanetary consequences caused by the extremely intense solar activity during October–November 2003, *J. Geophys. Res.*, *110*, A01109, doi:10.1029/2004JA010656.

Venkatakrishnan, P., and B. Ravindra (2003), Relationship between CME velocity and active region magnetic energy, *Geophys. Res. Lett.*, *30*(23), 2181, doi:10.1029/2003GL018100.

Vourlidas, A., D. Buzasi, R. A. Howard, and E. Esfandiari (2002), *Solar Variability: From Core to Outer Frontiers*, *ESA SP-506*, vol. 1., edited by A. Wilson, p. 91, ESA Publ. Div., Noordwijk.

Webb, D. F., C.-C. Cheng, G. A. Dulk, S. F. Martin, S. McKenna-Lawlor, D. J. McLean, and S. J. Edberg (1980), Mechanical energy output of the 5 September 1973 flare, in *Skylab Solar Workshop II*, edited by P. Sturrock, p. 471, Colo. Univ. Assoc. Press, Boulder, Colo.

Yashiro, S., N. Gopalswamy, G. Michaek, O. C. St.Cyr, S. P. Plunkett, N. B. Rich, and R. A. Howard (2004), A catalog of white light coronal mass

ejections observed by the SOHO spacecraft, *J. Geophys. Res.*, *109*, A07105, doi:10.1029/2003JA010282.

N. Gopalswamy, M. L. Kaiser, and S. Yashiro, NASA Goddard Space Flight Center, Greenbelt, MD 20771, USA. (gopals@fugee.gsfc.nasa.gov; yashiro@cdaw.gsfc.nasa.gov)

R. A. Howard and A. Vourlidas, Solar Physics Branch, Space Sciences Division, Naval Research Laboratory, Washington, DC 20375, USA. (russ.howard@nrl.navy.mil; vourlidas@nrl.navy.mil)

Y. Liu, W.W. Hansen Experimental Physics Laboratory, HEPL Annex, B210, Stanford University, Stanford, CA 94305-4085, USA. (yliu@quake.stanford.edu)

G. Michalek, Astronomical Observatory of Jagiellonian University, Orla 171, 30-244 Krakow, Poland. (michalek@oa.uj.edu.pl)

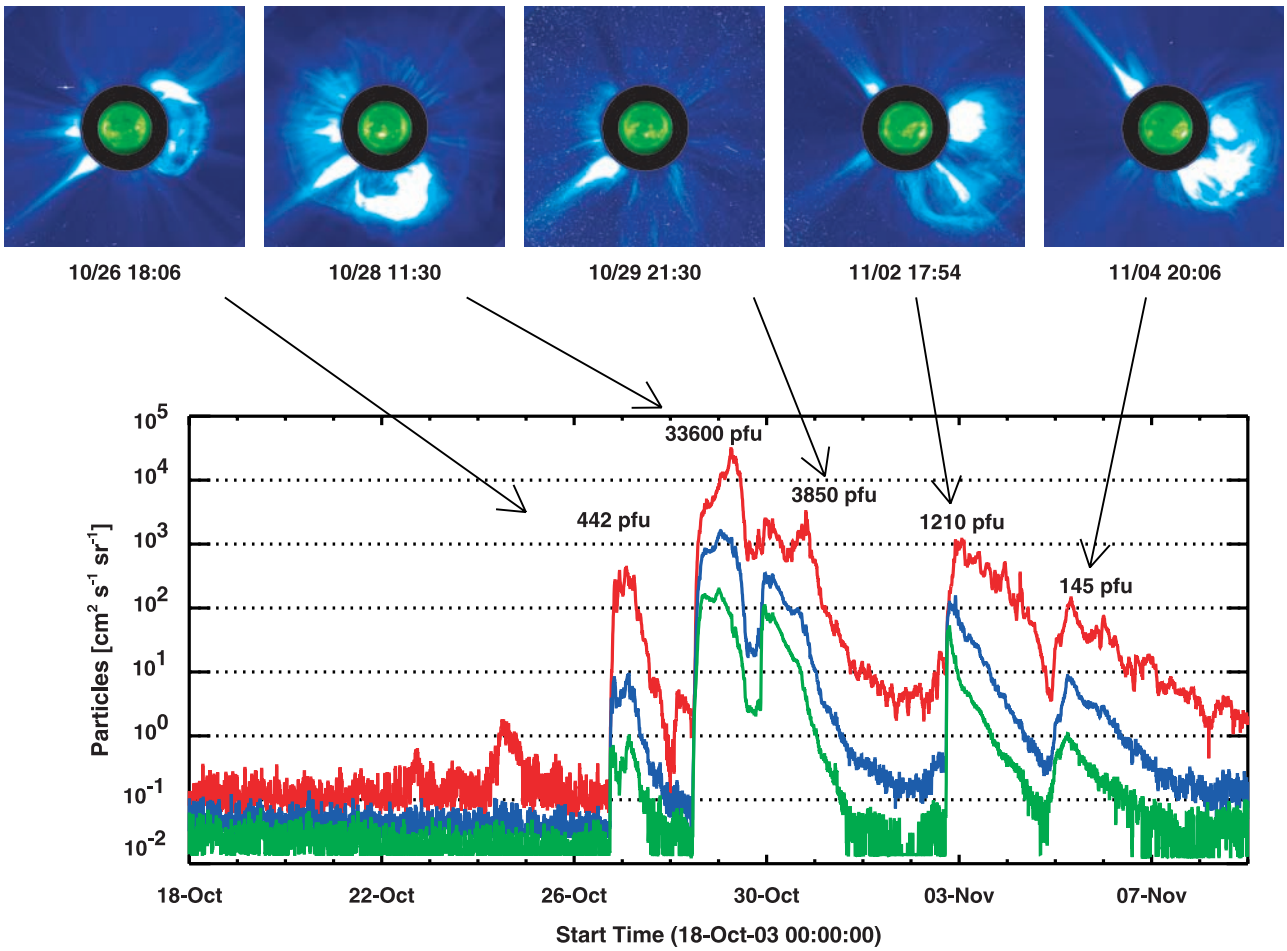

Figure 9. GOES proton intensity from 18 October 18 to 9 November 2003 showing several large SEP events. The peak values of the SEP intensity in the >10 MeV channel are indicated on the plots. The three plots represent the three energy channels: >10 MeV (red), >50 MeV (blue), and >100 MeV (green). The corresponding SOHO/LASCO CMEs are also shown. The bright compact regions in the SOHO/EIT images are the flaring regions. There is also another SEP event on 2 November at 1100 UT before the 1570 pfu event.

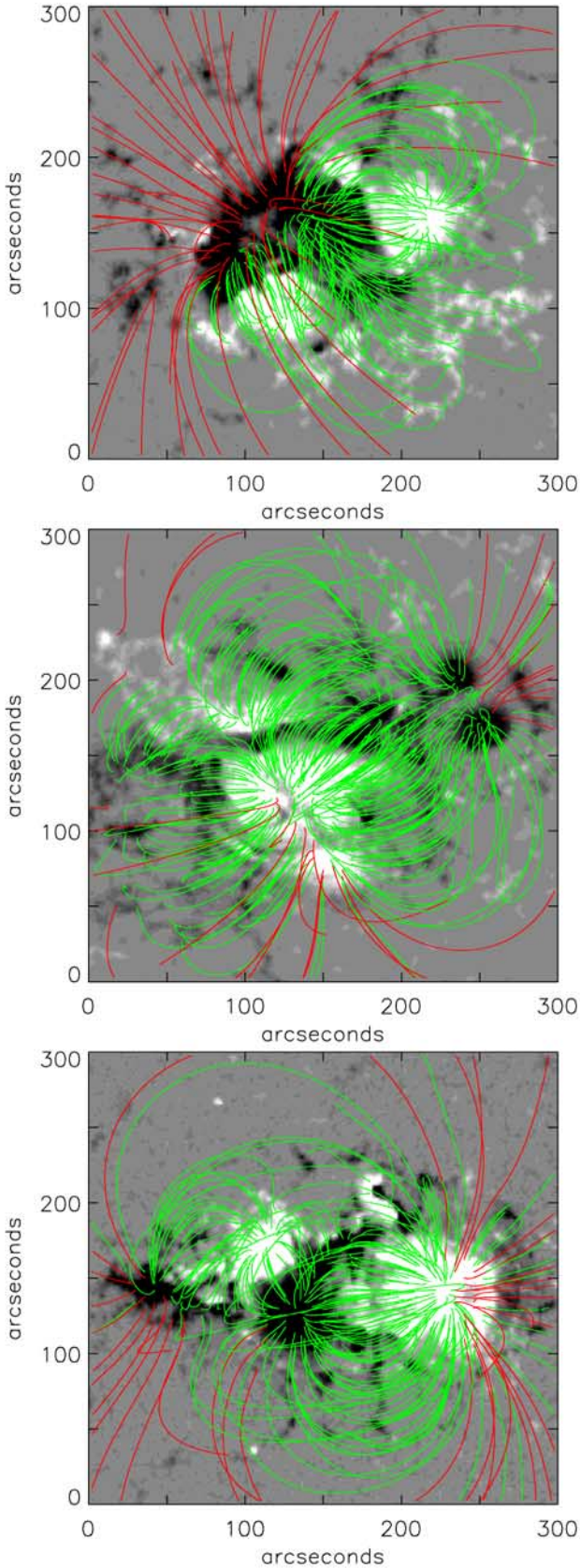

Figure 11. Selected magnetic field line computed by potential field extrapolation of the SOHO/MDI magnetograms for the three active regions: 484 (top), 486 (middle), and 488 (bottom). Green lines represent closed field lines, while the red shows the field lines running out of the cube.